



**Luis Miguel Lima de
Almeida**

Processamento ótico baseado em ótica integrada

All-optical processing based on integrated optics



**Luis Miguel Lima de
Almeida**

Processamento ótico baseado em ótica integrada

All-optical processing based on integrated optics

Dissertação apresentada à Universidade de Aveiro para cumprimento dos requisitos necessários à obtenção do grau de Mestre em Engenharia Eletrónica e Telecomunicações, realizada sob a orientação científica do Dr. António Teixeira, Professor do Departamento de Eletrónica, Telecomunicações e Informática da Universidade de Aveiro

Dissertation submitted to the University of Aveiro in the fulfilment of the requirements for the degree of Master in Electronics and Telecommunications Engineering, under the supervision of Doctor António Teixeira, Professor in the Department of Electronics, Telecommunications and Informatics of the University of Aveiro.

Dedico este trabalho à minha família pelo apoio prestado em toda a formação acadêmica.

o júri / the jury

Presidente / president

Professor Doutor Armando Humberto Moreira Nolasco Pinto
Professor associado da Universidade de Aveiro

Vogais / examiners committee

Professor Doutor António Luís Jesus Teixeira
Professor associado com agregação da Universidade de Aveiro (orientador)

Doutor Carlos Miguel Santos Vicente
Investigador de Pós Doutoramento do Instituto de Telecomunicações da Universidade de Aveiro

**Agradecimentos/
Acknowledgements**

I wish to thank to my supervisor Doctor António Teixeira for his orientation, guidance and encouragement during this work. I would also like to thank to Dr. Giorgia Parca, Dr. Naresh Kumar, Ana Lopes and professor Uwe Kahler for the help, advice and guidance during this work. It was a pleasure to work with all of them.

I wish to express a special gratitude for the financial support given by the CITO project PTDC/EEA-TEL/114838/2009 and to the Telecommunications Institute for all the support provided.

Last, but not least, my warm thanks to my family, girlfriend and friends for their love, help and understanding throughout my life. I would not have come so far without them.

palavras-chave

Ótica integrada, transformada de onduletas, transformada de onduletas de Haar, compressão de imagem, acoplador, Waveshaper, Matlab.

resumo

Nos últimos anos, a procura por elevados ritmos de transferência de informação em comunicações óticas tem aumentado exponencialmente. Dado que imagem, no seu formato original exactamente como é captada pela câmara fotográfica ocupa enormes quantidades de espaço de armazenamento, torna-se importante desenvolver um sistema que aumente o seu grau de compressão, preservando as informações importantes da imagem. No tópico da compressão de imagem existem várias técnicas de transformação usadas para compressão de dados. A transformada discreta de onduleta é uma das mais usadas, graças ao uso da transformação em multi-resolução. Esta propriedade de multi-resolução permite não só desenvolver métodos de compressão de imagem sem perdas, nos quais se obtém a imagem original exactamente como era antes da transformação, como também métodos com perdas, já não sendo possível obter a imagem original. Neste contexto, esta tese irá desenvolver a ideia de aplicar a transformada de onduleta de Haar usando circuitos óticos. Este conceito irá ser analisado, verificando a possibilidade da sua implementação no domínio ótico, usando vários métodos, com perdas e sem perdas, para concluir acerca do melhor método de compressão a aplicar a uma imagem. Por fim, o método com perdas irá ser testado no laboratório com diferentes componentes e desenhar o dispositivo ótico capaz de aplicar a transformada de onduleta de Haar.

keywords

Integrated optics, wavelet transforms, Haar wavelet transform, image compression, coupler, Waveshaper, Matlab.

abstract

During the last years, the demand for high data transfer rates in optical fiber communications has increased exponentially. Since image in its original format exactly as it is captured by the digital camera requires an enormous amount of storage capacity, it is important to develop a system that increases its amount of compression while preserving the important image's information.

In the topic of image's compression, there are several transformation techniques used for data compression. Discrete Wavelet Transform (DWT) is one of the most commonly used, thanks to its multi-resolution transformation. This multi-resolution property allows to develop, not only a lossless compression method, from which the original image can be obtained exactly as it was before the transform, but also, a lossy method where it is not possible to obtain the original image.

In this context, this thesis will develop the idea to apply the Haar wavelet transform using optical circuits. This concept will be analyzed, verifying the possibility of its implementation in the optical domain, using several methods, lossy and lossless, to conclude about the best compression method to apply to an image. Finally, the lossy method will be tested in the laboratory with different components and design the optical device able to accomplish the Haar wavelet transform.

Contents

Contents	i
List of Figures	iii
List of Tables	ix
Acronyms	xi
Chapter 1: Introduction	1
1.1 MOTIVATION	2
1.2 OBJECTIVES	2
1.3 THESIS ORGANIZATION	3
1.4 MAIN ACHIEVEMENTS	4
Chapter 2: Image compression	7
2.1 IMAGE COMPRESSION TRANSFORMATIONS METHODS	7
2.2 LOSSY VS LOSSLESS	7
2.3 IMAGE FORMATS	8
2.4 DISCRETE WAVELET TRANSFORM	9
2.4.1 Haar transform – based image compression system	10
2.4.2 Optical Haar transform device	12
2.5 IMAGE QUALITY ASSESSMENT PARAMETERS	15
Chapter 3: Theoretical implementation of the optical system in Matlab ...	19
3.1 IMPLEMENTATION OF THE HAAR WAVELET TRANSFORM	19
3.1.1 Lossless compression	21
3.1.2 Lossy compression	22
3.1.2.1 Lossy compression with variation in the amplitude of the parameters of the Haar transformation matrix	24
3.1.2.2 Lossy compression with variation in the phase of the parameters of the Haar transformation matrix	27
3.2 IMPLEMENTATION OF ADDITIONAL COMPRESSION IN THE DATA ENCODING PROCESS	30
3.2.1 Additional compression with threshold	30
3.2.2 Additional compression with quantization	32
Chapter 4: Laboratory experiment with the Haar wavelet transform	35
4.1 VISIBLE SPECTRAL REGION (635 NM WAVELENGTH)	35
4.1.1 Setup	35
4.1.2 Results	37
4.1.3 Image comparison	39
4.1.3.1 4x4 Image with moderate contrast:	39
4.2.3.2 4x4 Image with high contrast:	40
4.1.4 Discussion of results	41
4.2 C BAND (1550 NM WAVELENGTH)	41
4.2.1 Setup	42
4.2.2 Results	45
4.2.3 Image comparison	47
4.2.3.1 4x4 Image with moderate contrast:	47

4.2.3.2 4x4 Image with high contrast:.....	48
4.2.3.3 4x4 Image with low contrast:.....	49
4.2.3.4 8x8 Image with moderate contrast:.....	50
4.2.4 <i>Discussion of results</i>	51
Chapter 5: Optical Haar transform design	53
5.1 PHOENIX OPTODESIGNER	53
5.2 3dB ASYMMETRIC COUPLER DESIGN	53
5.3 OPTICAL HAAR TRANSFORM DESIGN	56
5.4 DISCUSSION OF RESULTS.....	58
Chapter 6: Conclusion and future work	63
References	65
Attachments	69

List of Figures

Figure 1: Data growth by year [2].	1
Figure 2: Process of a two level signal decomposition using multi-resolution analysis.	10
Figure 3: System building blocks for Haar optical wavelet transform (OWT) based on all-optical processing and compression. 2D transform process schematic describes low-pass (L) and high-pass (H) filtering until sub-band decomposition [16].	11
Figure 4: 3 dB asymmetric optical coupler scheme and scattering matrix [16].	13
Figure 5: 3D basic module for 1st-level optical 2D HT [16].	13
Figure 6: Integrated passive scheme for Optical WT-IWT; passive compression is accomplished by spatial selection of the LL coefficients, delivered through reported connections [16].	14
Figure 7: Haar wavelet transform applied to the image "TIF-1".	21
Figure 8: Size and image format comparison in lossless compression.	22
Figure 9: Size and image format comparison in lossy compression.	23
Figure 10: Compression ratio and file format of the image. Comparison by compression method.	24
Figure 11: MSE and amplitude variation in the Haar transform matrix comparison.	25
Figure 12: PNSR and amplitude variation in the Haar transform matrix comparison.	26
Figure 13: Quality and amplitude variation in the Haar transform matrix comparison.	27
Figure 14: MSE and phase variation in the Haar transform matrix comparison.	28
Figure 15: PNSR and phase variation in the Haar transform matrix comparison.	29
Figure 16: Quality and phase variation in the Haar transform matrix comparison.	29
Figure 17: Number of occurrences of each pixel (symbol) by level of threshold	31

Figure 18: Number of occurrences of each pixel (symbol) by level of quantization	33
Figure 19: Image 4x4 with moderate contrast.	35
Figure 20: Image 4x4 with high contrast.....	35
Figure 21: Setup with a 3dB coupler.	37
Figure 22: Photography of the 635 nm setup.	37
Figure 23: Theoretical Scaling image.	39
Figure 24: Obtained Scaling image from scheme 1 with IL.	39
Figure 25: Obtained Scaling image from scheme 1 without IL.	39
Figure 26: Obtained Scaling image from scheme 2 with IL.	40
Figure 27: Obtained Scaling image from scheme 2 without IL.	40
Figure 28: Theoretical Scaling image.	40
Figure 29: Obtained Scaling image from scheme 3 with IL.	41
Figure 30: Obtained Scaling image from scheme 3 without IL.	41
Figure 31: Image 4x4 with moderate contrast [22].	42
Figure 32: Image 4x4 with high contrast [22].	42
Figure 33: Image 4x4 with low contrast [22].	42
Figure 34: Image 8x8 with moderate contrast [22].	42
Figure 35: Setup with 3dB coupler.	44
Figure 36: Photography of the 1550 nm setup with 3dB coupler.....	44
Figure 37: Setup with Waveshaper.	44
Figure 38: Photography of the 1550 nm setup with Waveshaper.....	45
Figure 39: Theoretical Scaling image [22].	47
Figure 40: Obtained Scaling image from the 3dB coupler with IL.....	47
Figure 41: Obtained Scaling image from the 3dB coupler without IL [22].	47
Figure 42: Obtained Scaling image from the Waveshaper with IL.....	48
Figure 43: Obtained Scaling image from the Waveshaper without IL.....	48
Figure 44: Theoretical Scaling image [22].	48
Figure 45: Obtained Scaling image from the 3dB coupler with IL.....	48
Figure 46: Obtained Scaling image from the 3dB coupler without IL [22].	48
Figure 47: Obtained Scaling image from the Waveshaper with IL.....	49
Figure 48: Obtained Scaling image from the Waveshaper without IL.....	49
Figure 49: Theoretical Scaling image [22].	49
Figure 50: Obtained Scaling image from the 3dB coupler with IL.....	49

Figure 51: Obtained Scaling image from the 3dB coupler without IL [22].	49
Figure 52: Obtained Scaling image from the Waveshaper with IL.	50
Figure 53: Obtained Scaling image from the Waveshaper without IL.	50
Figure 54: Theoretical Scaling image [22].	50
Figure 55: Obtained Scaling image from the 3dB coupler with IL.	51
Figure 56: Obtained Scaling image from the 3dB coupler without IL [22].	51
Figure 57: Obtained Scaling image from the Waveshaper with IL.	51
Figure 58: Obtained Scaling image from the Waveshaper without IL.	51
Figure 59: 3 dB asymmetric coupler geometry and design [22].	54
Figure 60: Schematic of the optical Haar transform [22].	57
Figure 61: Power propagation along the optical Haar transform schematic for Experiment 1 [22].	60
Figure 62: Phase propagation along the optical Haar transform schematic for Experiment 1 [22].	61
Figure 63: TIF 1 - Original image.	69
Figure 64: TIF 1 - Haar transform image.	69
Figure 65: TIF 1 - Scaling image of the Haar transform.	69
Figure 66: TIF 2 - Original image.	69
Figure 67: TIF 2 - Haar transform image.	69
Figure 68: TIF 2 - Scaling image of the Haar transform.	69
Figure 69: TIF 3 - Original image.	70
Figure 70: TIF 3 - Haar transform image.	70
Figure 71: TIF 3 - Scaling image of the Haar transform.	70
Figure 72: TIF 4 - Original image.	70
Figure 73: TIF 4 - Haar transform image.	70
Figure 74: TIF 4 - Scaling image of the Haar transform.	70
Figure 75: JPEG 1 - Original image.	71
Figure 76: JPEG 1 - Haar transform image.	71
Figure 77: JPEG 1 - Scaling image of the Haar transform.	71
Figure 78: JPEG 2 - Original image.	71
Figure 79: JPEG 2 - Haar transform image.	71
Figure 80: JPEG 2 - Scaling image of the Haar transform.	71
Figure 81: JPEG 3 - Original image.	72
Figure 82: JPEG 3 - Haar transform image.	72

Figure 83: JPEG 3 - Scaling image of the Haar transform.	72
Figure 84: JPEG 4 - Original image.....	72
Figure 85: JPEG 4 - Haar transform image.	72
Figure 86: JPEG 4 - Scaling image of the Haar transform.	72
Figure 87: BMP 1 - Original image.	73
Figure 88: BMP 1 - Haar transform image.....	73
Figure 89: BMP 1 - Scaling image of the Haar transform.	73
Figure 90: BMP 2 - Original image.	73
Figure 91: BMP 2 - Haar transform image.....	73
Figure 92: BMP 2 - Scaling image of the Haar transform.	73
Figure 93: BMP 3 - Original image.	74
Figure 94: BMP 3 - Haar transform image.....	74
Figure 95: BMP 3 - Scaling image of the Haar transform.	74
Figure 96: BMP 4 - Original image.	74
Figure 97: BMP 4 - Haar transform image.....	74
Figure 98: BMP 4 - Scaling image of the Haar transform.	74
Figure 99: PNG 1 - Original image.	75
Figure 100: PNG 1 - Haar transform image.....	75
Figure 101: PNG 1 - Scaling image of the Haar transform.	75
Figure 102: PNG 2 - Original image.	75
Figure 103: PNG 2 - Haar transform image.....	75
Figure 104: PNG 2 - Scaling image of the Haar transform.	75
Figure 105: PNG 3 - Original image.	76
Figure 106: PNG 3 - Haar transform image.....	76
Figure 107: PNG 3 - Scaling image of the Haar transform.	76
Figure 108: PNG 4 - Original image.	76
Figure 109: PNG 4 - Haar transform image.....	76
Figure 110: PNG 4 - Scaling image of the Haar transform	76
Figure 111: Haar inverse transform from image TIF 1 after a threshold level of 0	77
Figure 112: Haar inverse transform from image TIF 1 after a threshold level of 4	77
Figure 113: Haar inverse transform from image TIF 1 after a threshold level of 8	77

Figure 114: Haar inverse transform from image TIF 1 after a threshold level of 16	77
Figure 115: Haar inverse transform from image TIF 1 after a threshold level of 32	78
Figure 116: Haar inverse transform from image TIF 1 after a threshold level of 64	78
Figure 117: Haar inverse transform from image TIF 1 after a threshold level of 128	78
Figure 118: Haar inverse transform from image TIF 1 after a quantization level of 1	78
Figure 119: Haar inverse transform from image TIF 1 after a quantization level of 2	79
Figure 120: Haar inverse transform from image TIF 1 after a quantization level of 5	79
Figure 121: Haar inverse transform from image TIF 1 after a quantization level of 10	79
Figure 122: Haar inverse transform from image TIF 1 after a quantization level of 20	79
Figure 123: Haar inverse transform from image TIF 1 after a quantization level of 50	80

List of Tables

Table 1: Characteristics of the images used for comparison.	20
Table 2: Quality assessment parameters by level of threshold	32
Table 3: Quality assessment parameters by level of quantization.....	34
Table 4: Power range used with the 3dB coupler setup.	36
Table 5: Schemes comparison for the 635 nm wavelength.....	38
Table 6: Power range used with the 3dB coupler setup.	43
Table 7: Power range used with the Waveshaper setup.	43
Table 8: Insertion loss and average Standard Deviation comparison.....	45
Table 9: MSE and PSNR comparison.	46
Table 10: Parameters for the simulated 3dB asymmetric coupler.	56
Table 11: Output values from the simulated 3db asymmetric coupler [22].	56
Table 12: Parameters for the optical Haar transform schematic.....	58
Table 13: Input and theoretical output value in each port of the optical Haar transform.	59
Table 14: Theoretical and output value in each port of the optical Haar transform.	60

Acronyms

1D	One-dimensional space
2D	Bi-dimensional space
A/m	Amplitude per meter
BMP	Bitmap Image File (.bmp)
Bpp	Bits per pixel
CMT	Coupled Mode Theory
dB	Decibels
dBm	Decibel milliwatts
DCT	Discrete Cosine Transform
DFT	Discrete Fourier Transform
DWT	Discrete Wavelet Transform
ECL	External Cavity Lasers
IL	Insertion Loss
JPEG	Joint Photographic Experts Group (.jpg)
kB	Kilobyte
MSE	Mean Square Error
mW	milliwatt
Nm	Nanometers
OWT	Optical Wavelet Transform
PNG	Portable Network Graphics (.png)
PSNR	Peak Signal to Noise Ratio
RGB	Red, Green, and Blue (primary colors)
ROI	Region of Interest
TE	Transverse Electric mode
TIF	Tagged Image File Format (.tiff)
TLS	Tunable Laser Source
WHT	Walsh Hadamard Transform
μm	Micrometers

Chapter 1: Introduction

“The real voyage of discovery consists not in seeking
new landscapes, but in having new eyes”

Marcel Proust

It is said that a picture is worth a thousand words. However, in this modern internet age, the demand for data transmission and data storage is increasing. As seen in Figure 1, the data growth is about 40% every year, reaching nearly 45 Zettabytes by the year 2020. Study has shown that the 90% of total volume of data in internet access consists of image and video related data [1], making this field of study very important to reduce that amount of data. Image in their *raw* (uncompressed) format requires huge storage space. Such *raw* data needs large transmission bandwidth for the transmission over the network. Hence, many researchers have been conducted in the field of data compression system.

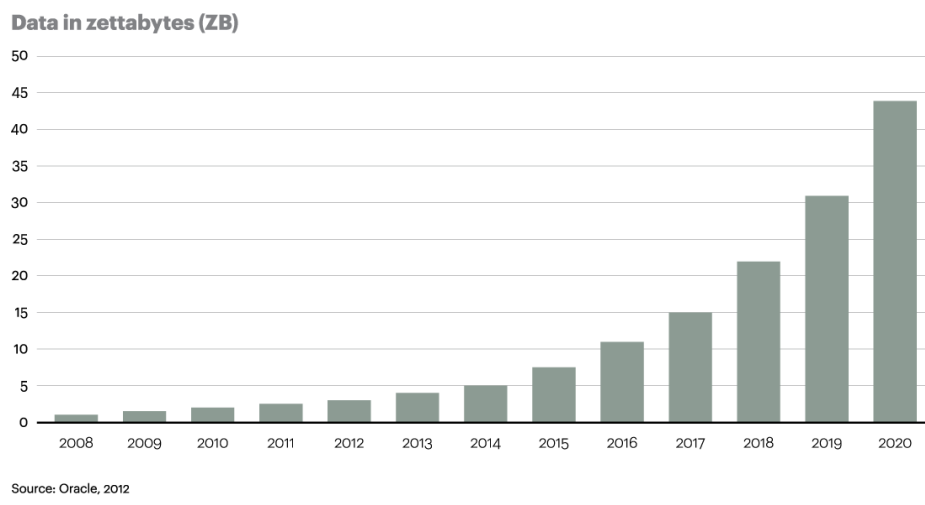


Figure 1: Data growth by year [2].

Compression techniques reduces the size of data, which in turn, requires less bandwidth, less transmission time and related cost. For that, they use compression algorithms, which assume that there is some bias on the input message of the data, so that some inputs are more likely than others. Most algorithms base this “bias” on the structure of the message, that there is some unbalanced probability distribution over the possible messages [3]. There are

algorithms developed for the data compression such as Discrete Cosine Transform (DCT), Discrete Wavelet Transform (DWT), Walsh Hadamard Transform (WHT), etc.

1.1 Motivation

Optical circuitry has recently become a very active research field due to the massive amount of real-time data via limited bandwidth channels. The advantage of optics is its capability of providing high count of parallel operations in a three dimensional space.

Some work has already been developed so far on the field of data processing using transforms. For example, on free-space optics using the Fourier transform as described in [4] or wavelet based models for propagation in optical fibers accordingly to [5]. In addition, the medical and security/encryption fields have shown a lot of interest in image compression due to the lack of secure and fast optical transmission channels, as presented in [6], [7] and [8].

Image compression suffers from large computational requirements. These types of data have to be compressed during the transmission process. Techniques that previously dominated the field such as Fourier transforms now have to compete with many other integral transforms and in particular with wavelet transforms. Wavelet analysis is a particular time or space scale representation of signals, which has found a wide range of applications in signal processing, physics and applied mathematics. 2D discrete wavelet transform (DWT) has been the most relevant, emerging image compression approach in such a way that it was adopted as the JPEG2000 standard [9].

1.2 Objectives

In this thesis, an all-optical processor based on integrated optics is presented. The two dimensional Discrete Wavelet Transform (DWT) will be applied on the data block of an image to implement a compression method. To begin with,

different compression methods will be studied: lossy compression, lossless compression, with threshold and with quantization. Then, a small part of the DWT image will be retrieved, the so called “Scaling image”, to study the possibility of a lossy compression method between optical devices in different wavelengths. If the compression method proves to be successful, the aim of the work will be deviated to the implementation of the complete DWT with the device Finisar Waveshaper 4000s, creating a lossless compression method.

The main objective of this thesis is to investigate the performance of the proposed all-optical processing based on integrated optics for wide range of image formats and applications.

1.3 Thesis organization

This thesis is organized in a clear and concise way for the reader to understand it in the simplest way possible:

Chapter 2: Image compression - For a better understanding of the following chapters, a brief explanation about image compression will be given in this chapter, starting with image compression transform methods. After that, a comparison between lossy and lossless compression will also be done, right after an explanation about Discrete Wavelet Transform, the image formats that will be used in this work and the most important subject of analysis. Related to it, the Haar wavelet transform and optical device will be explained. To finish with in this chapter, the image quality assessment parameters used will be defined.

Chapter 3: Theoretical implementation of the Haar wavelet transform - In this chapter, the Haar wavelet transform will be implemented and analyzed using the software Matlab, comparing different compression methods (lossy and lossless) and parameters variation in the Haar transform matrix. Two additional methods will also be studied, using the lossless compression method. An amount of threshold or quantization is applied to reduce the number of symbols in the image, increasing the data transmission speed.

Chapter 4: Laboratory experiment with the Haar wavelet transform - In this chapter, the Haar wavelet transform will be applied in the laboratory with two wavelengths, using real devices to check the practical use of the Haar transform when some errors are introduced. To begin with, a lossy compression method will be used. Then, if the lossy compression method proves to be successful, the focus will be moved to a lossless compression method using the component Finisar Waveshaper 4000s.

Chapter 5: Optical Haar transform design - In this chapter, an optical Haar transform will be designed and simulated using the software OptoDesigner. The refractive index of some materials used in the manufacturing of optical fiber circuits will be used, making it possible to build the device in the future.

Chapter 6: Conclusion and future work - In this chapter, the main conclusions of the previous chapters will be presented, as well as a perspective of the points that might be improved in the future, thus continuing the work developed so far.

1.4 Main achievements

With the work developed in this thesis, the following achievements were accomplished:

- All-optical system based on the Haar Wavelet transform capable of obtaining significant compression ratio with low loss of quality in image files;
- The setup with the 3dB coupler for the C band, has shown to provide images with high compression ratio and quality;
- With the design of the optical Haar transform, an optical device that performs successfully a lossy compression method based on the Haar wavelet transform;
- A publication in ICTON 2014:

L. Almeida, A. Teixeira, G. Parca, N. Kumar, A. Lopes, A. Tavares, A.

Shahpari, "All-Optical Image Compression Processing Based on Integrated Optics", 16th International Conference on Transparent Optical Networks, IEEE, 2014.

Chapter 2: Image compression

2.1 Image compression transformations methods

Image is digitally represented in a group of pixels. Usually the neighboring pixels are correlated to each other and are redundant in the image. The redundancy occupies unnecessarily storage space, which decreases the transmission speed and the bandwidth of the system.

Therefore, the aim is to reduce the redundancy of an image. The reduction in redundancy can be achieved by means of image compression techniques. The main idea behind the compression technique is to use orthonormal transformation making the pixel value smaller than the original. The transformation of the image also makes the coefficients of the transformed matrix uncorrelated with each other. There are various transformations being used for data compression:

- Discrete Fourier Transform (DFT);
- Walsh Hadamard Transform (WHT);
- Discrete Cosine Transform (DCT);
- Discrete Wavelet Transform (DWT).

There is a wide variety of wavelet-based image compression algorithms besides the Haar wavelet transform that will be focused in this thesis.

A new algorithm that used wavelet transform, which is embedded and minimizes the loss in image quality, is described in [10]. Many other algorithms are cited in article [11].

2.2 Lossy vs Lossless

There are two types of image compression: lossless and lossy.

Lossless compression uses as advantage the redundancy in the image and through efficient coding allows the reconstruction of the original image after decompression exactly as it was. As mentioned in [12], with images of natural scenes it is rarely possible to obtain error-free compression at a rate beyond 2:1. Unfortunately, lossless compression can become sensitive to bit errors in the

communications link and requires a certain amount of overhead to ensure no loss of data.

Much higher compression ratios can be obtained if some error, which is usually difficult to perceive, is allowed between the decompressed image and the original image. This is lossy compression. In some cases, it is not necessary that the original image not has errors to be reproduced, for example, in fast transmission of still images over the Internet.

Lossy compression techniques allows an increase of compression ratio with a cost of image quality. Usable lossy compression ratio range is from 4 or 5 with minimal image degradation, and from 40 or 50 with image quality that may still be adequate for qualitative interpretation [13], making important the choice of compression technique and ratio, and the resulting impact on the data is very dependent upon the system characteristics. Transform techniques, like the wavelet transform that will be used here, achieve compression by truncating and quantizing the number of coefficients and basis function used to represent the image.

To begin with, the focus will be on wavelet-based lossy compression of grayscale still images.

2.3 Image formats

Digital images need a file format that holds the digital image data securely and permanently. The file format is fundamental to the preservation and compression of an image.

There are some algorithms that perform this compression in different ways. Some are lossless and keep the same information as the original image, others lose information while compressing the image. Some of these compression methods are designed for specific kinds of images, so they will not be so good for others. Some algorithms even let you change the parameters they use, to better adjust the compression to the image.

The image formats that will be used in the course of this work are:

- BMP (bitmap) is a lossless bitmapped graphics format used commonly as a simple graphics file format on Microsoft;
- JPG is a lossy compression method, widely used in digital cameras and over the internet. Today, JPG is rather unique in this regard. Lossy compression allows very small files of lower quality, overcoming almost any other lossless file type;
- TIF is lossless, which is considered the highest quality format for commercial work. The TIF format is not necessarily any "higher quality" by itself (the image pixels are what they are). This simply means there are no additional losses or artifacts to degrade and detract from the original;
- PNG is a lossless compression method, invented more recently than the others, and since it is more modern, it offers additional options (RGB color modes, 16 bits ...). Other feature of PNG is transparency for 24 bit RGB images. Normally PNG files are smaller than TIF or GIF (both use different methods of lossless compression), but PNG is slightly slower to read or write.

2.4 Discrete Wavelet Transform

Wavelets are localized waves, whose main purpose is dropping to zero instead of oscillating forever as other transforms [14]. Wavelets produce a natural multi-resolution of every image (Scaling image), including all the important edges (details images).

Unlike the Fourier transform, the wavelet transform has the ability to capture both low pass and high pass behaviors of an image. This property has proved very useful in image compression. From an image compression point of view, computational efficiency is an important factor to be considered. Fortunately, unlike DCT, DWT can be implemented as a fast algorithm via subband coding scheme. Typically, Discrete Wavelet Transform starts with the lowest scale (lowest level), corresponding to the given image, and computes the DWT coefficients by iterating the filtering and subsampling processes. This results in one approximation and many detail coefficients, as seen in Figure 2. It has been

observed in [15] from examples, that most of the energy of the DWT coefficients is packed in the approximation coefficients, which is a factor in achieving higher compression.

The Discrete Wavelet Transform represents an image as a sum of wavelet functions, known as wavelets, with different location and scale [15]. It represents the data into a set of high pass (detail) and low pass (approximate) coefficients. The input data is passed through set of low pass and high pass filters as described in Figure 2.

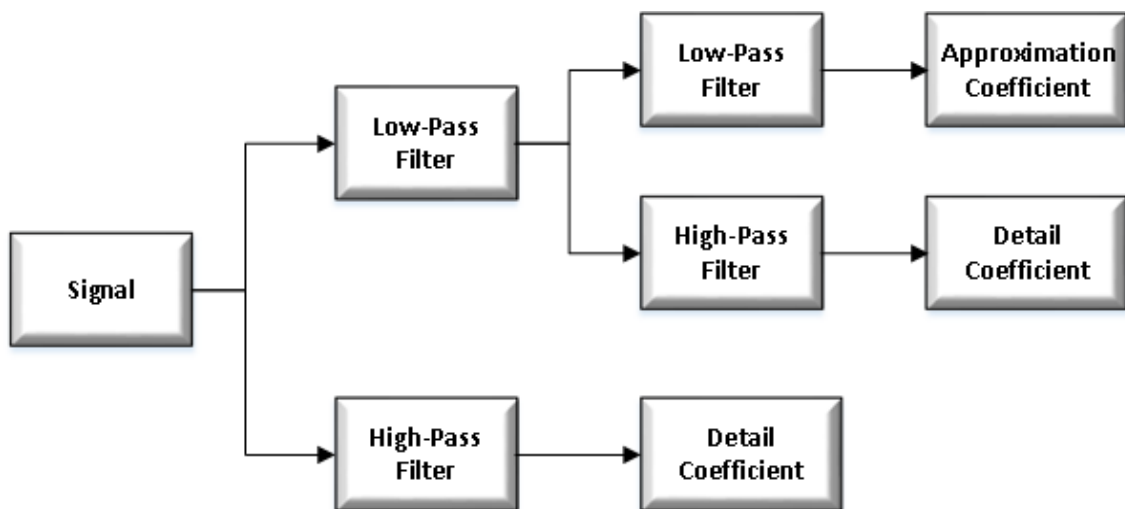


Figure 2: Process of a two level signal decomposition using multi-resolution analysis.

2.4.1 Haar transform – based image compression system

In order to fulfill the purpose of this thesis, the focus will be the Haar wavelet transform, also known as Daubechies D2 wavelet, presenting an all-optical image processing scheme based on it. The Haar wavelet transformation is an example of multi-resolution analysis. The purpose of this thesis is to use the Haar wavelet basis to compress an image data using the method of averaging and differencing to construct it. The simple Haar wavelet transformation matrix is given by Equation (2.1):

$$\text{Haar transformation matrix} = \begin{bmatrix} \frac{1}{\sqrt{2}} & \frac{1}{\sqrt{2}} \\ \frac{1}{\sqrt{2}} & -\frac{1}{\sqrt{2}} \end{bmatrix} \quad (2.1)$$

The system and building blocks used to process image were based on the described system building blocks and equations reported in [16] and [17], demonstrated in Figure 3.

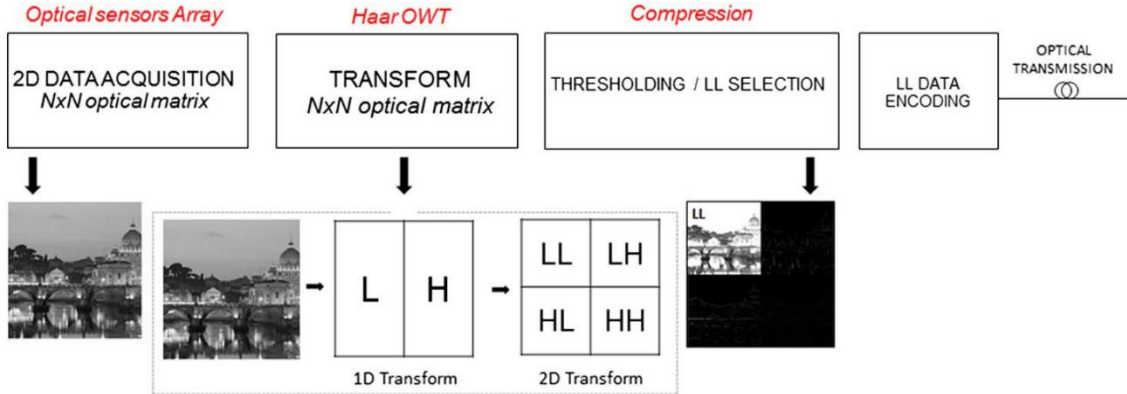


Figure 3: System building blocks for Haar optical wavelet transform (OWT) based on all-optical processing and compression. 2D transform process schematic describes low-pass (L) and high-pass (H) filtering until sub-band decomposition [16].

The system described in Figure 3 is a Haar all-optical wavelet transform (OWT), allowing fast image processing, with four main blocks:

- Optical sensors array: this is the first building block, the acquisition stage with optical sensors for light detection and 2D data sampling to obtain an optical input data matrix with the same size $N \times N$ of the original image;
- Haar OWT: the second building block will be responsible for applying the Haar transform to the image $N \times N$ obtained in the previous block, extracting the image properties obtained from exploiting the energy compaction features of wavelet decomposition. In this block, a matrix $N \times N$ will be applied based on Equation (2.2), the corresponding Haar Transform scattering matrix for a generic 1D input (a_i coefficients), which might be one pixel line or pixel column. This matrix includes the low-pass (L) and high-pass (H) filters associated with the Haar wavelet, that will be applied two times, one to obtain the 1D Transform (L and H component), and another to obtain the desirable 2D Transform with the four resulting

components, LL, LH, HL and HH. The resulting coefficients on the left side of Equation (2.2) are the scaling c_{ij} and detail d_{ij} coefficients (being i the transform level and j the coefficients index) obtained from the low-pass and high-pass filtering, respectively, of each pixel pair, and corresponding to the 1D first level Haar discrete wavelet transform;

$$\begin{bmatrix} \vdots \\ c_{10} \\ d_{10} \\ c_{11} \\ d_{11} \\ c_{12} \\ d_{12} \\ \vdots \end{bmatrix} = \frac{1}{\sqrt{2}} \begin{bmatrix} \dots & \dots & \dots & \dots \\ 1 & 1 & 0 & 0 & 0 & 0 & \dots \\ 1 & -1 & 0 & 0 & 0 & 0 & \dots \\ 0 & 0 & 1 & 1 & 0 & 0 & \vdots \\ \vdots & \vdots & \vdots & \vdots & \vdots & \vdots & \vdots \\ 0 & 0 & 1 & -1 & 0 & 0 & \vdots \\ 0 & 0 & 0 & 0 & 1 & 1 & \vdots \\ 0 & 0 & 0 & 0 & 1 & -1 & \dots \\ \dots & \dots & \dots & \dots & \dots & \dots & \dots \end{bmatrix} \begin{bmatrix} \vdots \\ a_0 \\ a_1 \\ a_2 \\ a_3 \\ a_4 \\ a_5 \\ \vdots \end{bmatrix} \quad (2.2)$$

- Compression: the aim of the third block is to compress and extract the desirable information from the 2D transform. In this block, the data will be quantized, reducing precision and specific components will be extracted, for example, the LL component;
- LL data encoding: the last block will adapt the image data for the optical channel, compressing the data coding and bit stream formation.

On the receiver, after the optical channel, an inverse system will perform all the inverse transforms provided by the blocks on Figure 3, decoding the bit stream, de-quantized and then apply the inverse Haar transform on the data, returning the image able to be displayed.

2.4.2 Optical Haar transform device

To accomplish the Haar transform, the optical device choice must be one that accomplishes the scattering matrix from Equation (2.1), averaging and differentiating each optical input pair, as seen in Figure 4. Knowing that, the chosen device was a monomode 3dB asymmetric coupler, also known as Magic-T. An asymmetric coupler is a coupler with different waveguide widths, which might have a wide range of coupling ratios and low value of excess loss (0.7dB), including input and output single-mode fiber coupling losses [18]. In the case of

this thesis, since the asymmetric coupler must be arranged with not only a 50% coupling ratio, but also a phase difference between waveguides, a waveguide-type optical π hybrid coupler will be designed according to [16] and [19].

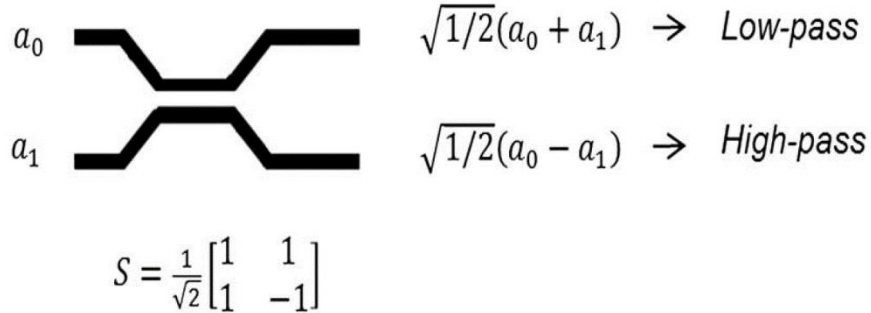


Figure 4: 3 dB asymmetric optical coupler scheme and scattering matrix [16].

Starting from the principle displayed in Figure 4 for a 1D transform, a 2D transform device will be designed, creating a three dimensional basic module, as shown in Figure 5. This device will implement the Low and High filtering one dimension a time, producing the scattering matrix given by Equation (2.2). From a 2 by 2 input matrix, with coefficients a_0, a_1, a_2 and a_3 , the first two Magic-T will produce the first high-pass and low-pass filtering along one dimension, the horizontal values. After this, the values will pass again by other two Magic-T, applying again the high-pass and low-pass filtering along the other dimension, the vertical values. With this, the scaling coefficients c_{ij} and detail coefficients d_{ij} will be obtained, corresponding to the first level Haar DWT.

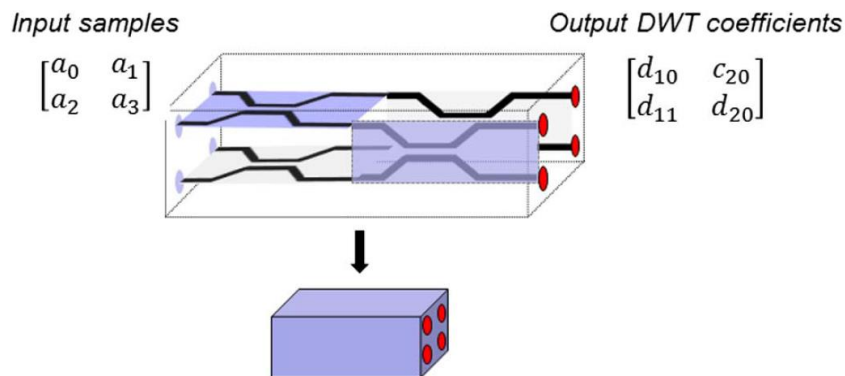


Figure 5: 3D basic module for 1st-level optical 2D HT [16].

In this case of 2D processing, i is related to the filtering step on each dimension, while j is, again, the coefficients index.

With the device from Figure 5, the input data set can be increased, pilling and joining the basic module, creating a three dimensional integrated passive scheme for all-optical DWT with size $N \times N$ as shown in Figure 6. Figure 6 describes an 8 by 8 data input performing a second level wavelet transform.

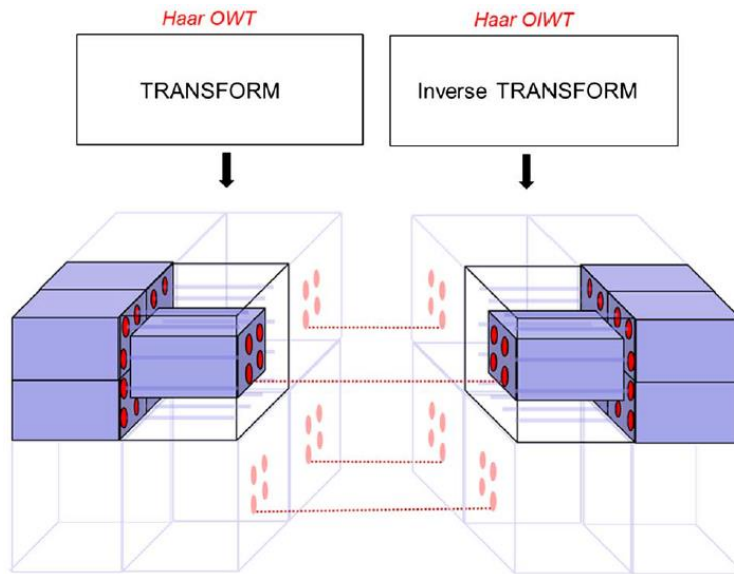


Figure 6: Integrated passive scheme for Optical WT-IWT; passive compression is accomplished by spatial selection of the LL coefficients, delivered through reported connections [16].

For this device, only lossy compression method was considered, discarding some of the components and delivering to the Inverse transform block a reduced amount of information selected through a compression criterion.

Since the human eye is more sensitive to contrast changes while keeping the brightness differences, than to color changes [21], applying the wavelet transform will allow selecting the portion of the spectrum more sensitive to the human eye, the low frequency (LL) component. Reducing or eliminating the high frequency components will allow it to obtain compression, while keeping the most relevant information for the human eye.

Therefore, in order to implement compression, the possibility of using lossy compression will be considered, delivering only the lower frequency (LL) components using a guided and passive scheme. This approach will be tested on the mathematical software Matlab, selecting only the LL components, the

same transform block described in Figure 6, where only the low-frequency coefficients will propagate along active connections (lossy compression), accomplishing a passive selection for compression purposes.

2.5 Image quality assessment parameters

For the purpose of image analysis, the following quality assessment parameters will be used in this work. The simplest and most widely used full-reference quality metrics are:

- **MSE:** the Mean Square Error is one way to evaluate the difference between an obtained value and the true value of the pixel obtained. MSE measures the average of the square of the error, with the error being the amount by which the estimator differs from the quantity to be estimated. The MSE between two images f and g is defined by Equation (2.3), in pixels:

$$MSE = \frac{1}{N} \sum_{j,k} (f[j, k] - g[j, k])^2 \quad (2.3)$$

Where the sum over j, k denotes the sum over all pixels in the images and N is the number of pixels in each image. The closer the value of the MSE is to zero, the smaller the value of the error is and more similar is the compressed image to the original;

- **PSNR:** In Peak Signal to Noise Ratio, the square of the peak value in the image is taken (in case of an 8-bit image, the peak value is 255) and divided by the Mean Square Error. The PSNR is used to measure the quality of an image after being submitted to a transformation. The PSNR between two (8 bpp) images is defined by Equation (2.4), in decibels (dB):

$$PSNR = 10 \log_{10} \left(\frac{255^2}{MSE} \right) \quad (2.4)$$

PSNR tends to be cited more often, since it is a logarithmic measure, and our brains seem to respond logarithmically to intensity. Increasing PSNR

represents increasing fidelity of compression. Generally, when the PSNR is between 30 dB and 40 dB, then the two images are virtually indistinguishable by human observers. When both images are identical (MSE of zero pixel), the PSNR is undefined, which in this case, to represent it graphically, the value of 99dB will be used.

These formulas are appealing because they are simple to calculate, have clear physical meanings, and are mathematically convenient in the context of optimization. However, they are not very well matched to perceived visual quality. For that, an additional quality assessment parameter will also be used:

- **Quality:** Universal Image Quality Index is a formula based on [20], which instead of using the traditional error summation methods, like MSE and PSNR, is designed by modeling the image distortion as a combination of loss correlation, luminance distortion and contrast distortion.

If $x = \{x_i\}$ is the original image and $y = \{y_i\}$ is the test image, with $i = \{1, 2, \dots, N\}$, the quality index is defined by Equation (2.5):

$$Quality = \frac{4\sigma_{xy}\bar{x}\bar{y}}{(\sigma_x^2 + \sigma_y^2)[(\bar{x})^2 + (\bar{y})^2]} \quad (2.5)$$

Where

$$\begin{aligned} \bar{x} &= \frac{1}{N} \sum_{i=1}^N x_i, & \bar{y} &= \frac{1}{N} \sum_{i=1}^N y_i, & \sigma_x^2 &= \frac{1}{N-1} \sum_{i=1}^N (x_i - \bar{x})^2, \\ \sigma_y^2 &= \frac{1}{N-1} \sum_{i=1}^N (y_i - \bar{y})^2, & \sigma_{xy} &= \frac{1}{N-1} \sum_{i=1}^N (x_i - \bar{x})(y_i - \bar{y}) \end{aligned}$$

The parameter Quality has a dynamic range from [-1, 1], with 1 being the best value where the obtained image is equal to the original and -1 being the lowest value achieved.

In evaluating the performance of any new image compression algorithm, one must take into account not only MSE, PSNR and Quality values, but also consider the following factors:

- Perceptual quality of the images (visual difference of the original image and the compressed image);
- Whether the algorithm allows for progressive transmission;
- The complexity of the algorithm (including memory usage);

- Whether the algorithm has ROI (Region of Interest) capability.

In addition, in order to compare the amount of compression obtained by a compression method, the size (occupied space on the hard drive) of two images will be compared, in this case, the compressed image and the uncompressed image. The parameter Compression Ratio will be given by Equation (2.6):

$$\text{Compression ratio} = \frac{\text{size of original image}}{\text{size of compressed image}} \quad (2.6)$$

In this case, if a compression ratio of 4 is obtained, the value is displayed “4:1”, which means that the compressed image is four times smaller than the original image.

Chapter 3: Theoretical implementation of the optical system in Matlab

3.1 Implementation of the Haar wavelet transform

To implement theoretically the Haar wavelet transform, the mathematical software MATLAB was used to compress and analyze the image data.

To do that, several types of images were used with different formats (TIF, JPEG, BMP and PNG), all of them square images with the same number of lines and columns (as seen in Chapter 2.4, the Haar transformation matrix is a square matrix) and all of them in the grayscale color space.

The reason to use only grayscale images was to simplify the analysis, since the main difference for this case, is that instead of having three colors like in the RGB color space (Red, Green and Blue), it has only one.

Finally, the reason to use four types of image formats was that all image formats (TIF, JPEG, BMP and PNG) are different: some lossless, other lossy, all with different characteristics that will differ after being affected by the Haar wavelet transform. This is important because in some cases, the transformation will be more significant and in other cases, the transformation will have much less effect. The characteristics of the images used in this chapter are listed in Table 1.

Name	Figure in Attachments	Format	Color space	Size (kB)	Size (Rows x Columns)
TIF - 1	Figure 63	TIF	Grayscale	265	512 x 512
TIF - 2	Figure 66	TIF	Grayscale	65	256 x 256
TIF - 3	Figure 69	TIF	Grayscale	1 040	1024 x 1024
TIF - 4	Figure 72	TIF	Grayscale	31	688 x 688
JPEG - 1	Figure 75	JPG	Grayscale	1 564	2832 x 1832
JPEG - 2	Figure 78	JPG	Grayscale	338	2832 x 2832
JPEG - 3	Figure 81	JPG	Grayscale	857	2832 x 2832
JPEG - 4	Figure 84	JPG	Grayscale	599	2832 x 2832
BMP - 1	Figure 87	BMP	Grayscale	263	512 x 512
BMP - 2	Figure 90	BMP	Grayscale	67	256 x 256
BMP - 3	Figure 93	BMP	Grayscale	41	200 x 200
BMP - 4	Figure 96	BMP	Grayscale	361	600 x 600
PNG - 1	Figure 99	PNG	Grayscale	61	300 x 300
PNG - 2	Figure 102	PNG	Grayscale	63	512 x 512
PNG - 3	Figure 105	PNG	Grayscale	483	1001 x 1001
PNG - 4	Figure 108	PNG	Grayscale	198	512 x 512

Table 1: Characteristics of the images used for comparison.

To start the Haar wavelet transform, an “Original image” with size $N \times N$, was multiplied 2 times by the “Haar transformation matrix” with size $N \times N$ (applied to the rows and column) to obtain the “Haar transform image”. The “Haar transform image” contains the “Scaling image”, “Horizontal details image”, “Vertical details image” and “Diagonal details image”, which in this step a lossless compression method is obtained, that means, it is possible to redo the transform and obtain the original image exactly as it was (first step of Figure 7).

To increase the amount of compression, with the “Haar transform image”, it is possible to extract the “Scaling image”, which is an image much similar to the original, but with size $\frac{N}{2} \times \frac{N}{2}$. In this case, the compression method is lossy, since from only the “Scaling image”, it is not possible to retrieve the original image.

The previous steps can be seen in Figure 7.

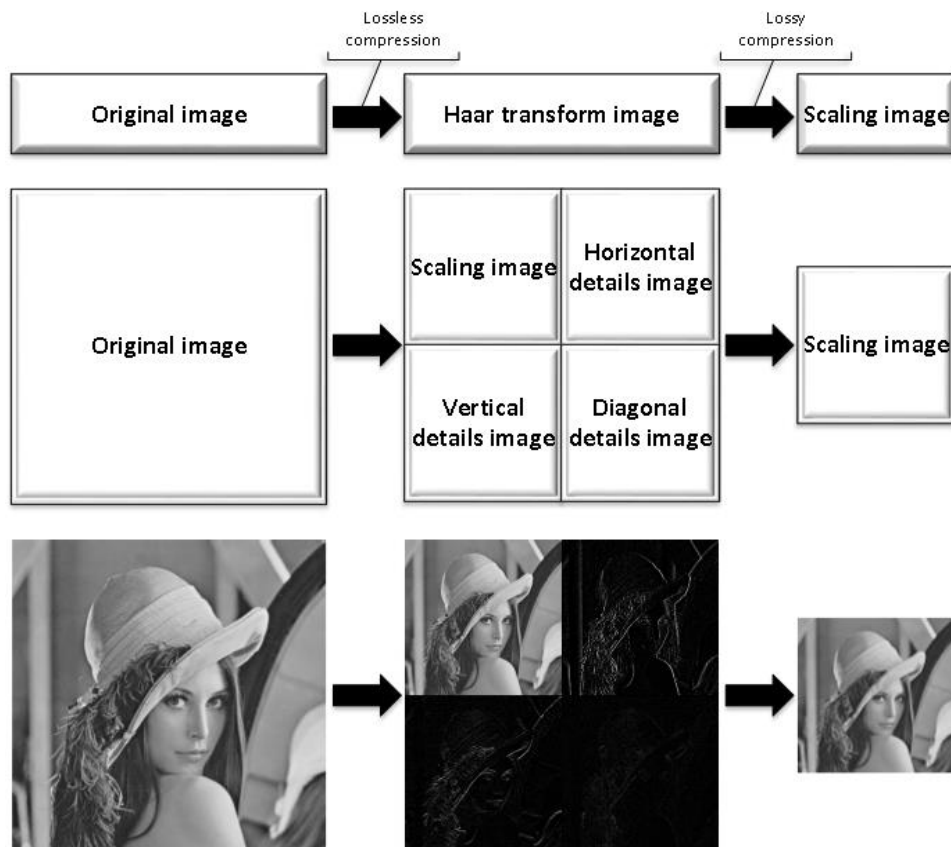


Figure 7: Haar wavelet transform applied to the image "TIF-1".

3.1.1 Lossless compression

To analyze the lossless compression method in Matlab, the size (occupied space on the hard drive) of the original image was compared with the resulting image of the Haar transform. The results can be seen in Figure 8.

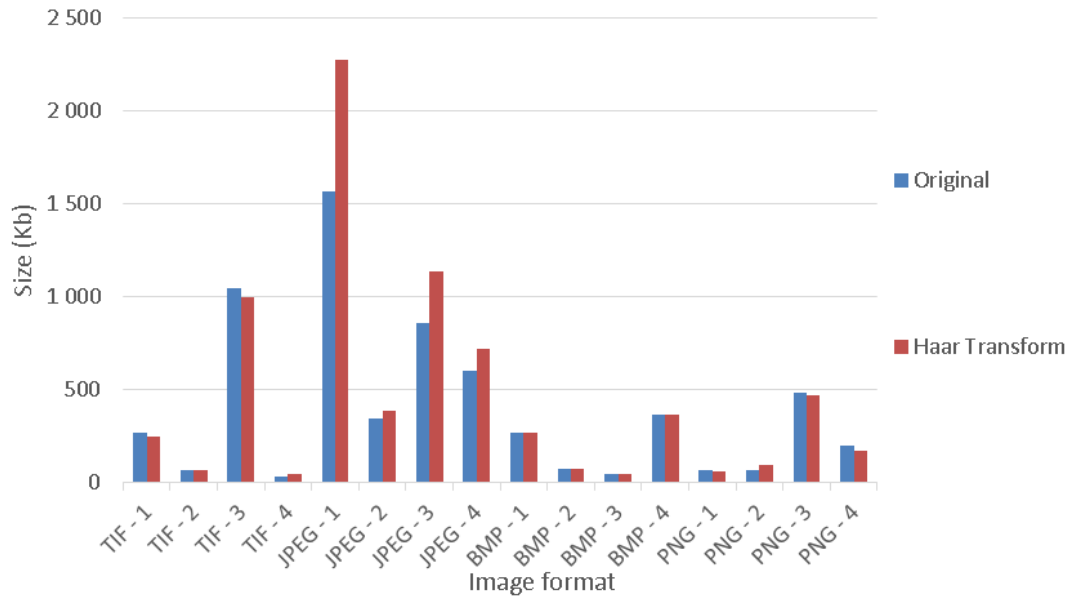


Figure 8: Size and image format comparison in lossless compression.

As seen in Figure 8, the lossless compression of the Haar transform might be useful in the lossless compression methods, like TIF, BMP and PNG, producing images approximately 8% smaller than the original. However, in the case of the JPEG lossy compression method, since the image was already highly compressed, the resulting image from the Haar transform is larger than the original, introducing redundancy in the output.

3.1.2 Lossy compression

After the lossless compression, the lossy compression method will be analyzed in Matlab, comparing the size (occupied space on the hard drive) of the original image with the Scaling image resulting from the Haar transform. The results can be seen in Figure 9.

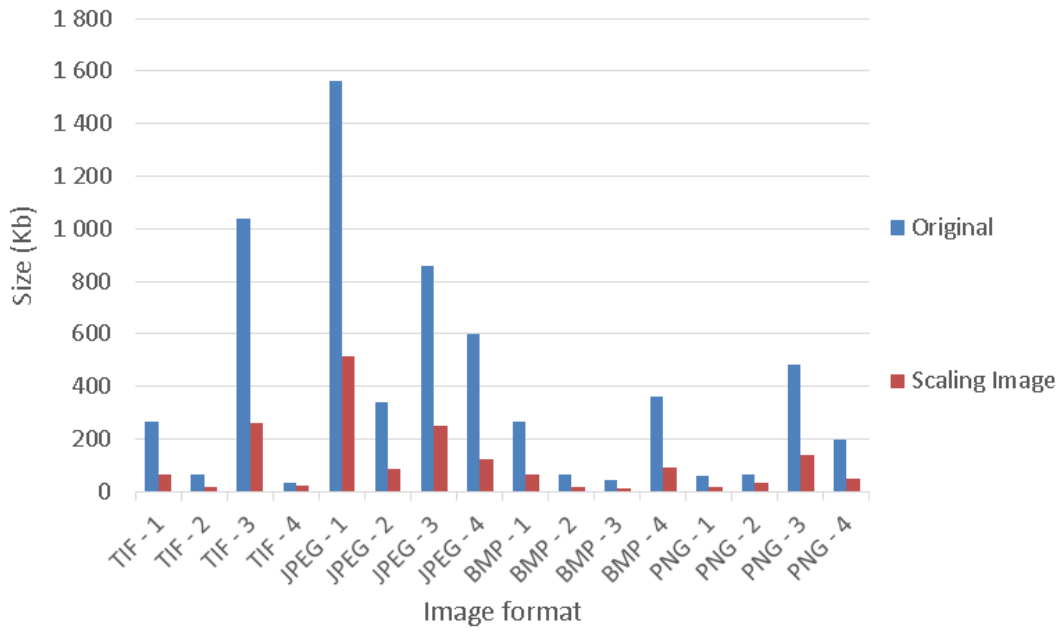


Figure 9: Size and image format comparison in lossy compression.

As seen in Figure 9, the lossy compression method of the Scaling image is able to compress all the image's formats, lossy or lossless, but with the cost of losing quality and a resulting image with half the rows and columns of the original image. In Figure 10, with the values from Figure 8 and Figure 9, the compression ratios of the Haar transform and Scaling image were calculated in order to visualize the amount of compression able to obtain with each one of the methods.

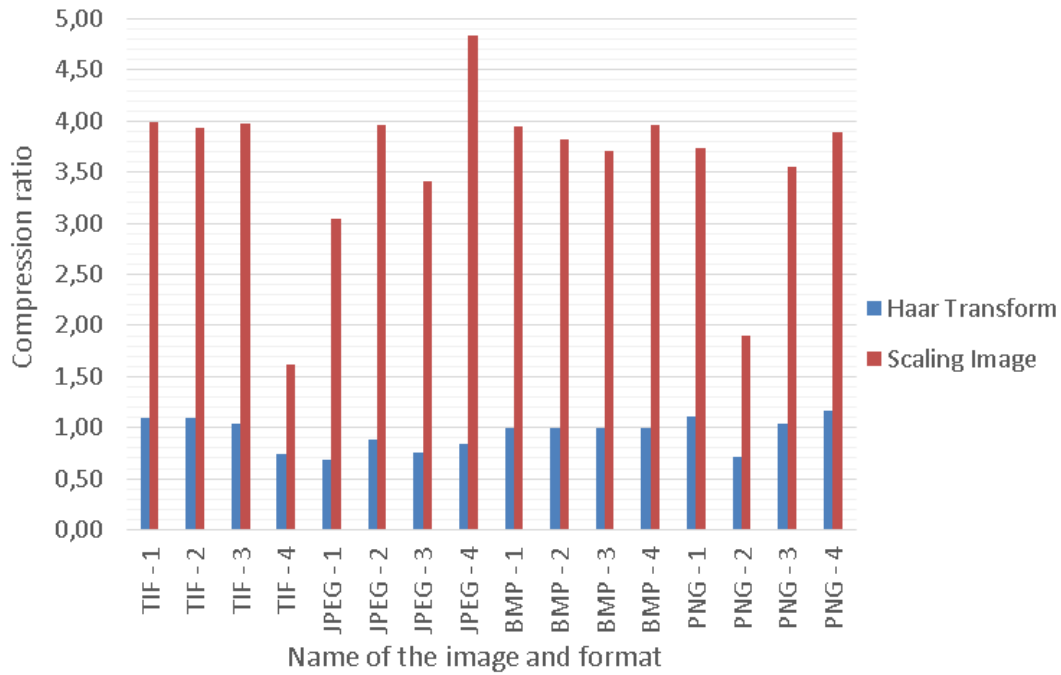


Figure 10: Compression ratio and file format of the image. Comparison by compression method.

From Figure 10, it is clear that with the lossy compression method of the Scaling image, it is possible to obtain an average compression ratio around 4:1 and with the lossless method of the Haar transform, the average compression ratio is about 1:1, which means that when the size of the image is not important, and high compression ratio is required, lossy compression method can be advantageous.

3.1.2.1 Lossy compression with variation in the amplitude of the parameters of the Haar transformation matrix

In this chapter, the amplitude of the Haar transformation matrix parameters were changed, in order to analyze the effect of loss in the parameters of a real device used in the laboratory, to obtain only the Scaling image.

Five different configurations were used to simulate the transformation, changing the amplitude from 0.088 to 1.1414. There is one configuration with all the parameters of Equation (3.1) changing in the same amplitude, and four configurations changing each one of the four parameters from Equation (3.1) and maintaining the remaining parameters from Equation (2.1) unchanged.

$$\text{Basic Haar transformation matrix} = \begin{bmatrix} 1^{st} & 2^{nd} \\ 3^{rd} & 4^{th} \end{bmatrix} \quad (3.1)$$

To compare the effect of the parameters, three image quality assessment parameters were used: MSE, PSNR and Quality, Figure 11, Figure 12 and Figure 13 respectively.

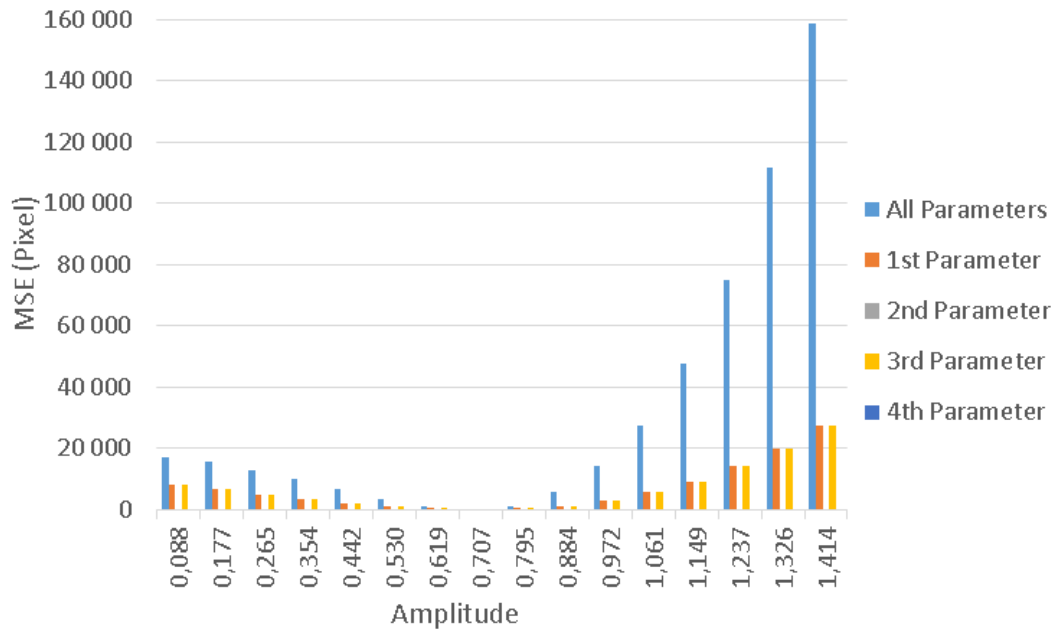


Figure 11: MSE and amplitude variation in the Haar transform matrix comparison.

In Figure 11, it is possible to observe that when it comes to the MSE, the most significant output is when all the parameters are affected by an error, obtaining the highest values of MSE. The other two parameters that affect the Scaling image are the first and the third parameters, still affecting considerably the output image outside the range of values between 0.530 and 0.884. The second or fourth parameter do not affect in any way the output of the Scaling image.

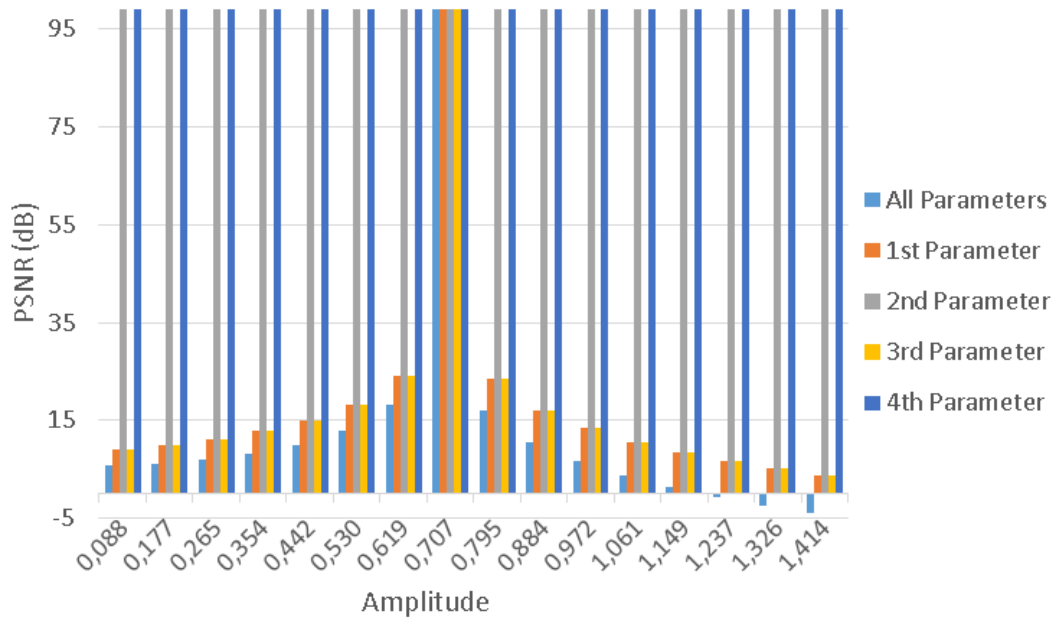


Figure 12: PNSR and amplitude variation in the Haar transform matrix comparison.

In Figure 12, it is possible to observe that the effect of the parameters on the PSNR is much likely as the effect on the MSE. When the second or forth parameters are affected or a value of $0.707 (\frac{1}{\sqrt{2}})$ is obtained, the Scaling image is not affected at all (PSNR of 99dB). If the values diverge from 0.707, increasing or lowering, the Scaling image is affected and the values of the PSNR start decreasing. The PSNR decreases more when all the parameters are affected.

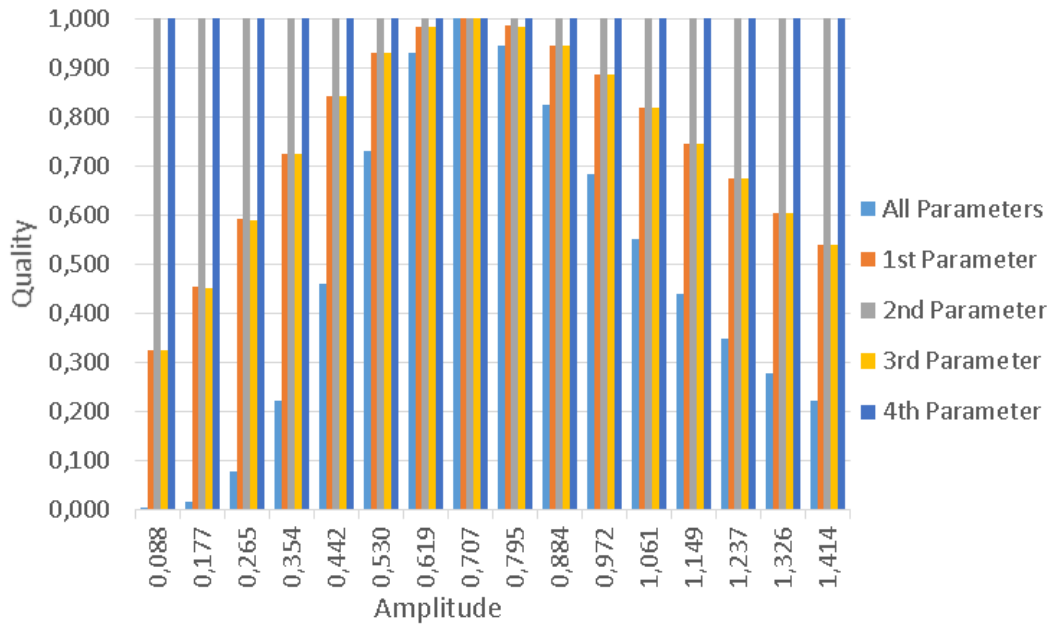


Figure 13: Quality and amplitude variation in the Haar transform matrix comparison.

Finally, in Figure 13, the deductions from Figure 11 and Figure 12 are verified, where besides the findings in the previous figures of MSE and PSNR, outside the range of values between 0.530 and 0.884, the Quality of the image decreases below 0.9, which is a significant perceptual difference in the Scaling image.

3.1.2.2 Lossy compression with variation in the phase of the parameters of the Haar transformation matrix

In this chapter, the phase of the Haar transformation matrix parameters were changed, in order to analyze the effect of loss in the parameters of a real device used in the laboratory.

Five different configurations were used to simulate, changing from -90 degrees to 90 degrees. There is one configuration with all the phase parameters of Equation (3.1) changing in the same amplitude of phase, and four configurations changing each one of the 4 parameters from Equation (3.1) and maintaining the remaining phase parameters from Equation (3.2) unchanged.

$$\text{Haar transformation matrix} = \begin{bmatrix} \frac{1}{\sqrt{2}} \cos(0^\circ) & \frac{1}{\sqrt{2}} \cos(0^\circ) \\ \frac{1}{\sqrt{2}} \cos(0^\circ) & \frac{1}{\sqrt{2}} \cos(180^\circ) \end{bmatrix} \quad (3.2)$$

To compare the effects, the same three image quality assessment parameters from the last chapter were used: MSE, PSNR and Quality, Figure 14, Figure 15 and Figure 16 respectively.

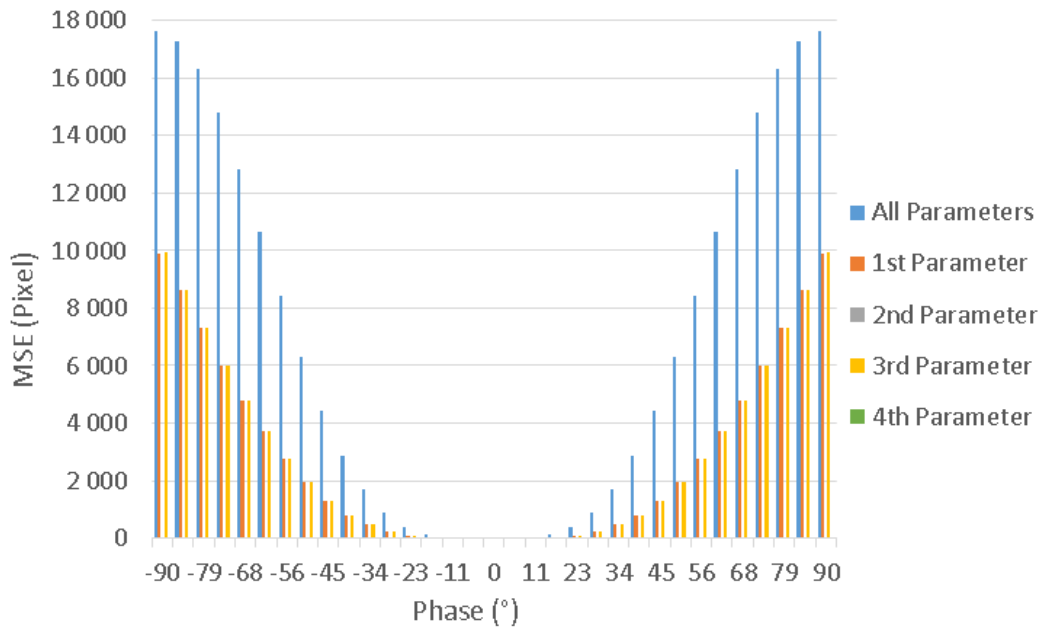


Figure 14: MSE and phase variation in the Haar transform matrix comparison.

In Figure 14, it is possible to observe that when it comes to the MSE, the most significant output is when all the parameters are affected by an error in the phase, obtaining the highest values of MSE. The other two parameters that affect the Scaling image are the first and the third parameters, still affecting considerably the output image outside the range of values between -45° and 45° . The second or fourth parameter do not affect in any way the output of the Scaling image.

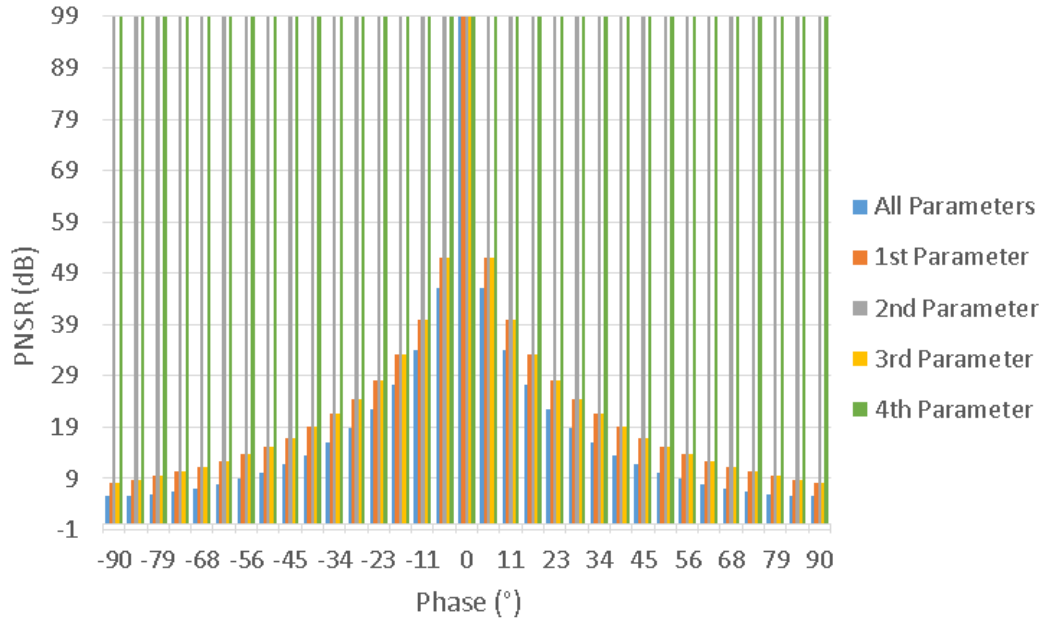


Figure 15: PSNR and phase variation in the Haar transform matrix comparison.

In Figure 15, it is possible to observe that the effect of the parameters on the PSNR is much likely as the effect on the MSE. When the second or forth parameter are affected or a phase difference of 0° is obtained, the Scaling image is not affected at all (PSNR of 99dB). If the phase diverges from 0° , increasing or lowering, the Scaling image is affected and the values of the PSNR start decreasing. The PSNR decreases more when all the parameters are affected.

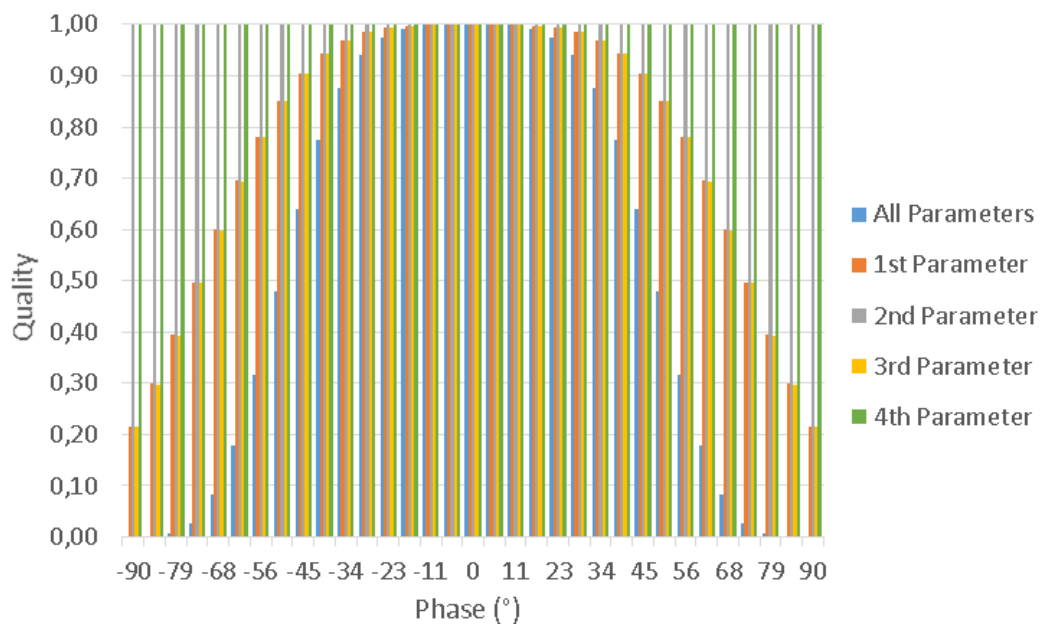


Figure 16: Quality and phase variation in the Haar transform matrix comparison.

Finally, in Figure 16, the deductions from Figure 14 and Figure 15 can be verified, where besides the findings in the previous figures of MSE and PSNR, outside the range of values between -45° and -45° , the Quality of the image decreases below 0.9, which is a significant perceptual difference in the Scaling image.

3.2 Implementation of additional compression in the data encoding process

As seen in Chapter 2.4, after the Haar transformation block, it is possible to increase the data transmission by a thresholding or quantization method before the optical transmission, where the number of symbols necessary to encode will be reduced, increasing the data transmission speed.

To analyze these methods, the mathematical software MATLAB was used to compress and analyze the image TIF 1 (Figure 63 from Attachments) after lossless compression: first by a thresholding method, then with a quantization method. The analysis was directed to the lossless compression due to the high quantity of zero values presented in the details coefficients in the Haar transform image (Figure 64 from Attachments), which is the one that will be transmitted in the optical transmission channel in this case.

3.2.1 Additional compression with threshold

In this part, additional compression will be added by a thresholding method.

Image threshold is a simple, yet effective way of reducing the number of symbols necessary to encode an image.

This method sets all the negative pixel, and below a certain amount threshold with the value zero. With this, the necessary symbols to encode those amounts were eliminated.

For example, an image with the pixel's values of 56, 200, 8 and 0, before thresholding, four sets of symbols were needed to encode that image (56, 200, 8

and 0). If a thresholding of 50 was applied, only three sets of symbols would be needed (56, 200, and 0), eliminating the symbol necessary to encode pixel 8. Seven levels of thresholding were used (0, 4, 8, 16, 32, 64 and 128), where in the first level (0) only the negative values were made equal to zero. In the remaining levels (4, 8, 16, 32, 64 and 128), they were already submitted to some amount of thresholding. For example, with the threshold level 8, the symbols necessary to encode the negative pixels and the pixels from 1 to 7 were eliminated.

The obtained images after applying the threshold 0, 4, 8, 16, 32, 64 and 128 can be seen in the chapter Attachment, Figure 111, Figure 112, Figure 113, Figure 114, Figure115, Figure 116 and Figure 117 respectively.

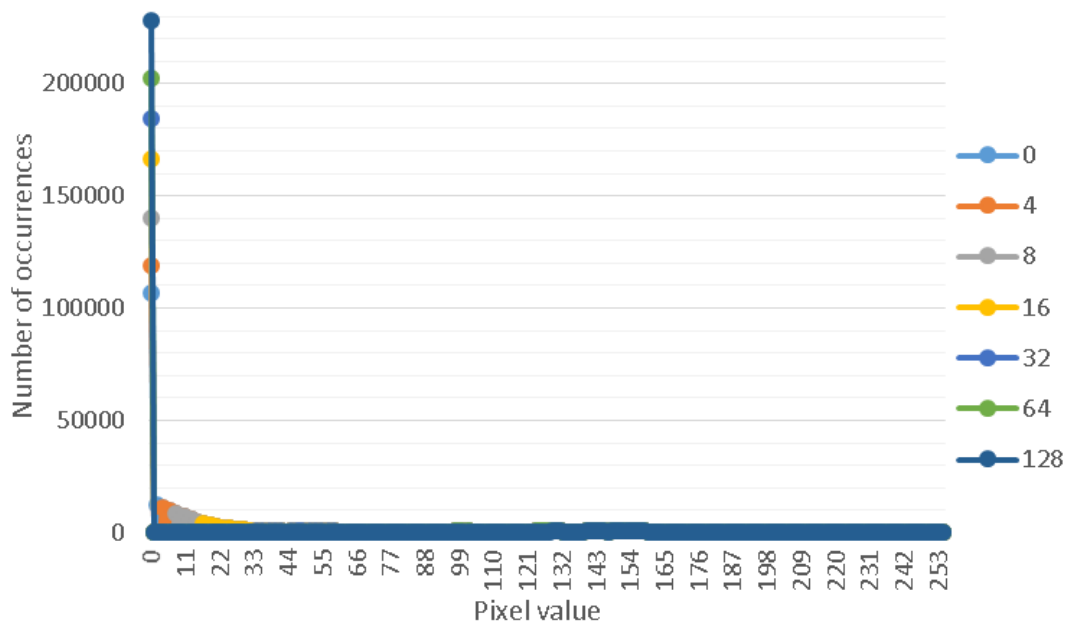


Figure 17: Number of occurrences of each pixel (symbol) by level of threshold

From Figure 17, it is possible to say that, higher the threshold submitted to the image, higher the number of occurrences of the value zero. In addition, while the threshold is increased, the lower values (threshold of 0, 4, 8 and 16) tend to lower exponentially the number of occurrences, which are the ones that are being turned into zero. By the analysis of this figure (17), the expected result is confirmed, which is a lower number of symbols in the image, turning the values lower than a threshold equal to zero.

Level of threshold	MSE (pixel)	PSNR (dB)	Quality
0	22.04	34.70	0.90
4	22.05	34.70	0.90
8	22.18	34.67	0.90
16	22.91	34.53	0.86
32	25.68	34.03	0.82
64	440.22	21.69	0.69
128	3976.00	12.14	0.37

Table 2: Quality assessment parameters by level of threshold

From Table 2 and the figures in the chapter Attachment (Figure 111, Figure 112, Figure 113, Figure 114, Figure 115, Figure 116 and Figure 117), until the threshold value of 32, the image does not show much loss of quality, obtaining a quality assessment parameters of 25.68 pixels for the MSE, 34.03 dB of PSNR and 0.82 of Quality. This method has proven to be a very good way to increase the data transmission speed of the Haar transform image in the optical transmission channel.

3.2.2 Additional compression with quantization

In this chapter, additional compression will be added by a quantization method. Image quantization is another simple way of reducing the number of symbols necessary to encode an image.

This method sets all the negative pixel equal to zero and the positive values are rounded to the nearest multiple of quantization's value. With this, the necessary symbols to encode those amounts were eliminated.

For example, an image with the pixel's values of 56, 200, 8 and 0, before quantization, four sets of symbols to encode that image were needed (56, 200, 8 and 0). If a quantization value of 100 was applied, only three sets of symbols would be needed (100, 200, and 0), eliminating the symbol necessary to encode pixel 8.

Six levels of quantization were used (1, 2, 5, 10, 20 and 50), where in the first level (1) only the negative values were made equal to zero. In the remaining levels (2, 5, 10, 20 and 50), they were already submitted to some amount of quantization. For example, from the quantization level 2, only approximately half of the symbols are needed to encode the image comparing to the quantization level 1.

The obtained images after applying the quantization 1, 2, 5, 10, 20 and 50 can be seen in the chapter Attachment, Figure 118, Figure 119, Figure 120, Figure 121, Figure 122 and Figure 123 respectively.

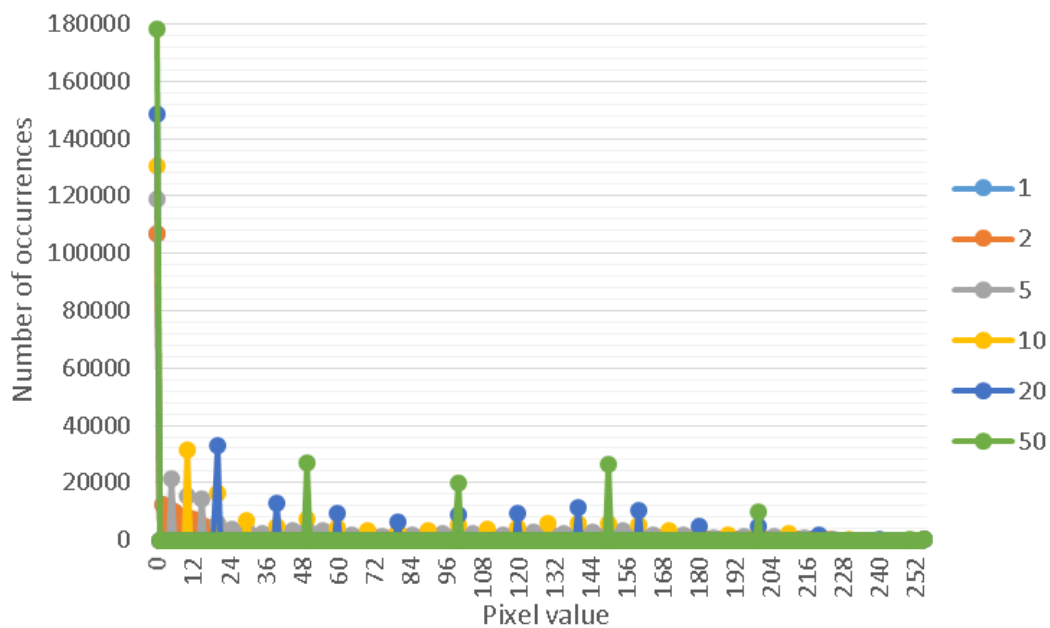


Figure 18: Number of occurrences of each pixel (symbol) by level of quantization

From Figure 18, it is possible to say that, higher the quantization submitted to the image, higher the number of occurrences of value zero, but still lower than the values obtained from the previous threshold method. Also, while the quantization value is increased, higher are the occurrences of the values along the horizontal scale of Figure 18. By the analysis of this figure, the expected result is confirmed, which is an increase of the values that are multiple to the quantization value, reducing the amount of symbols between two multiples of the quantization.

Level of quantization	MSE (pixel)	PSNR (dB)	Quality
1	21.86	34.73	0.90
2	22.25	34.66	0.90
5	23.91	34.35	0.86
10	30.45	33.29	0.77
20	55.94	30.65	0.65
50	198.21	25.16	0.39

Table 3: Quality assessment parameters by level of quantization

From Table 3 and the figures in the chapter Attachment (Figure 118, Figure 119, Figure 120, Figure 121, Figure 122 and Figure 123), until the quantization value of 5, the image does not show much loss of quality, obtaining a quality assessment parameters of 23.91 pixels for the MSE, 34.35 dB of PSNR and 0.86 of Quality. This method has proven to be a very good way to increase the data transmission speed of the Haar transform image in the optical transmission channel.

Chapter 4: Laboratory experiment with the Haar wavelet transform

In this chapter, the Haar Wavelet transform was simulated in the laboratory using the available devices. Two wavelength with distinct characteristics were chosen to verify the dependency of the wavelength in the experiment, with different optical lasers, components and measurement equipment.

The first wavelength used was the 635 nm, a visible red laser to the human observer. The second wavelength used was the 1550 nm, which, contrary to the wavelength of 635 nm, is not visible to the human eye.

4.1 Visible spectral region (635 nm wavelength)

To accomplish the experiment in the visible spectral region (635 nm), two small portions of the grayscale image “TIF-1” (Figure 63 from Attachments) were extracted, with a size of 4x4 pixel to compare in terms of contrast: one with moderate contrast and one with higher level of contrast, Figure 19 and Figure 20 respectively.

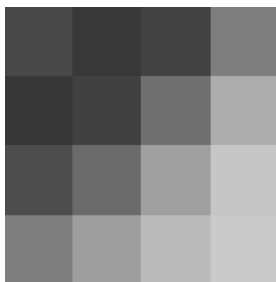


Figure 19: Image 4x4 with moderate contrast.

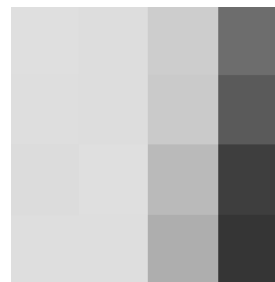


Figure 20: Image 4x4 with high contrast.

4.1.1 Setup

First, to start the experiment, the pixel value of the images were converted to a power scale (dBm), maximizing the power range available from the red lasers.

The ranges used in the experiment are listed in Table 4 for each one of the schemes used.

Unit \ Image		Moderate contrast image with Coupler 1 (scheme 1)	Moderate contrast image with Coupler 2 (scheme 2)	High contrast image with Coupler 2 (scheme 3)
Pixel	Lower value	55	55	53
	Higher value	202	202	223
dBm	Lower value	-24.1	-24.1	-24.0
	Higher value	-17.5	-17.5	-18.0

Table 4: Power range used with the 3dB coupler setup.

Secondly, two different setups with two different images were used to compare results. One of the setups (scheme 1) was assembled with a two input, two output 3dB coupler for the 635 nm wavelength with the following coupling coefficients:

- Input 1 – Output 1: 50.6%;
- Input 1 – Output 2: 49.4%;
- Input 2 – Output 1: 48.8%;
- Input 2 – Output 2: 51.2%.

The second setup (scheme 2 and scheme 3) was assembled with a different two input, two output 3dB coupler for the 635 nm wavelength with the following coupling coefficients:

- Input 1 – Output 1: 52.2%;
- Input 1 – Output 2: 47.8%;
- Input 2 – Output 1: 49.1%;
- Input 2 – Output 2: 50.9%.

The rest of the components were common to each one of the setups:

- 2 Red lasers with different power ranges;

- 1 Power meter.

The described setup can be seen in Figure 21 and Figure 22.

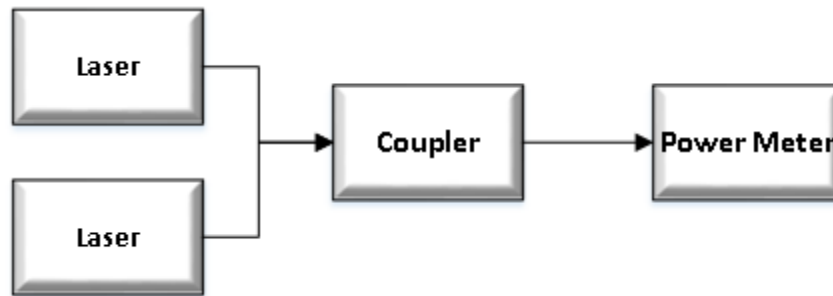


Figure 21: Setup with a 3dB coupler.

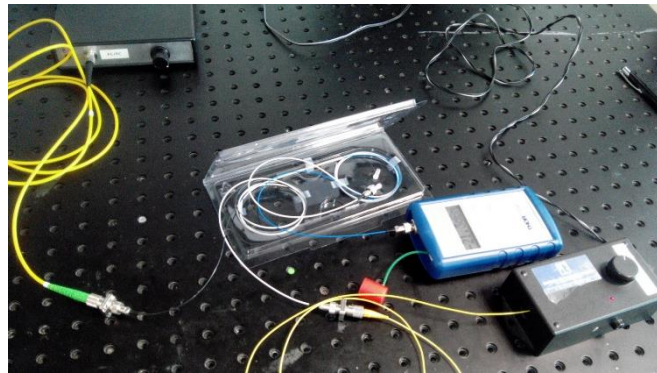


Figure 22: Photography of the 635 nm setup.

Next, with the pixel's values converted to the power scale (dBm):

- First, those values were regulated in the input of the 3dB coupler in groups of two horizontal values and obtained the vertical transform (L component of the Haar wavelet transform). The experiment was repeated 3 times;
- Secondly, the values obtained in the previous paragraph were adjusted again in groups of 2 vertical values, obtaining the final LL component (Scaling image of the Haar wavelet transform).

4.1.2 Results

To analyze the results, besides the parameters already discussed in Chapter 2.5, two more parameters were used regarding the experience in the laboratory:

- Insertion Loss (IL): an average parameter, obtained by dividing the obtained value of the pixels by their theoretical value. The meaning of this parameter is that since most of the components used in the laboratory have a percentage of loss in this operation, if the Insertion Loss is constant during the experiment, that value of loss is possible to compensate in the receiver canceling that loss. This value will be multiplied again by the obtained pixel to analyze the result of the component's loss in the experiment;
- Average Standard Deviation: an average value of the standard deviation calculated by discrepancy of the pixel in the output of the coupler in the repetition of the experiment 3 times. This parameter is used to verify the insertion of loss during the experiment while connecting and disconnecting the fibers. The lower the value obtained, the better the experiment will be.

	Insertion Loss (pixel)	Average Standard Deviation (pixel)	MSE (pixel)	PSNR (dB)
Scheme 1	7.95±12.33	1.99	9611.2	8.3
Scheme 1 with IL			9476.8	8.4
Scheme 2	26.19±61.93	4.69	10839.5	7.8
Scheme 2 with IL			10815.5	7.8
Scheme 3	71.35±168.58	2.42	26860	3.8
Scheme 3 with IL			4919	11.2

Table 5: Schemes comparison for the 635 nm wavelength.

From Table 5, looking to the obtained values of the parameter Insertion Loss, it is possible to say that the obtained pixel, even without considering the loss in the components, will be very different from the original values, since the minimum deviation is around 12 pixel. This results are verified in the obtained values of MSE and PSNR, where with or without considering the IL (Insertion Loss parameter), the MSE is extremely high and the PSNR is very low, expecting

images very different from the originals. From the values obtained in the Average Standard Deviation, in the case of the 635 nm wavelength, it is possible to say that, the process of connecting and disconnecting the fibers, introduces some error, from about 2 to 4 pixel.

4.1.3 Image comparison

In this chapter, the images will be compared using the human eye perception, comparing the theoretical Scaling image with each one of the obtained Scaling images. Two obtained Scaling images will be displayed, one that was multiplied by the obtained value of Insertion Loss to try to cancel the value of loss in the components (with IL) and other exactly as it was obtained (without IL).

4.1.3.1 4x4 Image with moderate contrast:

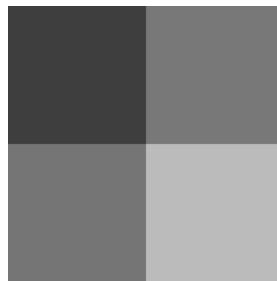


Figure 23: Theoretical Scaling image.

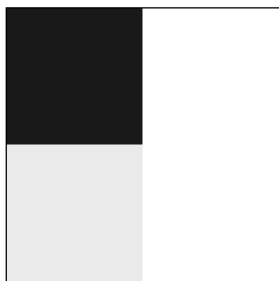


Figure 24: Obtained Scaling image from scheme 1 with IL.



Figure 25: Obtained Scaling image from scheme 1 without IL.

Comparing the theoretical Scaling image (Figure 23) with the obtained images (Figure 24 and Figure 25), it is possible to confirm the deductions made in chapter 4.1.2, where the images obtained with scheme 1 are both (with and without IL) very different from the theoretical, being the obtained image without IL the one with similar contrast but much darker.

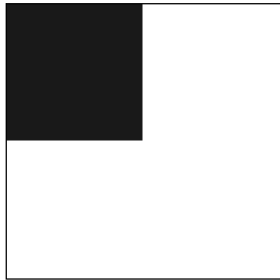


Figure 26: Obtained Scaling image from scheme 2 with IL.



Figure 27: Obtained Scaling image from scheme 2 without IL.

Looking to Figure 26 and Figure 27, the deductions made from Figure 24 and Figure 25 are also proven, where both images are very different from the theoretical.

4.2.3.2 4x4 Image with high contrast:

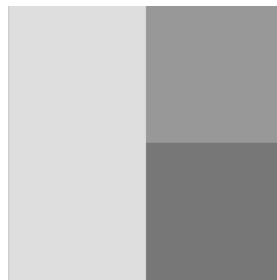


Figure 28: Theoretical Scaling image.

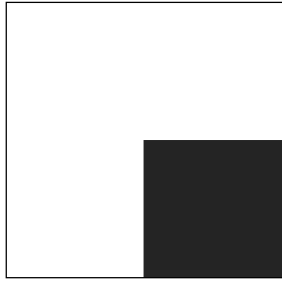


Figure 29: Obtained Scaling image from scheme 3 with IL.

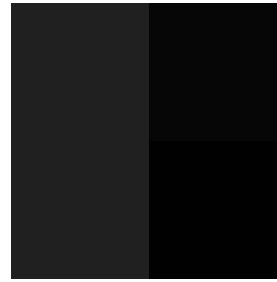


Figure 30: Obtained Scaling image from scheme 3 without IL.

From Figure 29 and Figure 30, the deductions made from the previous images (Figure 24, Figure 25, Figure 26 and Figure 27) remain the same, proving the previous conclusions.

4.1.4 Discussion of results

The laboratory experiment in the visible spectral region (635 nm wavelength) has proven to have a lot of error, making the obtained images very different from the expected ones. Some of the causes for this amount of error are:

- The power meter available for the wavelength 635 nm, had only one decimal value, becoming difficult to precise the value in the input and measure the correct output of the coupler;
- Since it was observed in Table 5 in the quality parameter Average Standard Deviation, the components are very sensitive to dust and dirt, and the operation of this experiment involved constantly connect and disconnect fibers, introducing significant amount of errors by doing that operation.

4.2 C band (1550 nm wavelength)

To accomplish the experiment in the C band (1550 nm wavelength), four small portions of the grayscale image “TIF-1” (Figure 63 from Attachments) were extracted with different sizes and contrasts. Three portions of the image with a size of 4 by 4 pixel were used to compare in term of contrast: one with moderate

contrast, another with high contrast and another with low contrast, as shown in Figure 31, Figure 32 and Figure 33 respectively. And finally, one portion with a size 8 by 8 pixel (Figure 34) was also used with a little bit of contrast to analyze the output when the image gets larger.

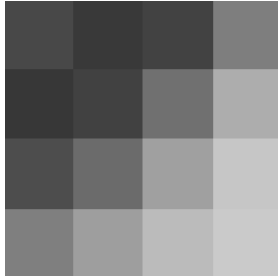


Figure 31: Image 4x4 with moderate contrast [22].



Figure 32: Image 4x4 with high contrast [22].



Figure 33: Image 4x4 with low contrast [22].



Figure 34: Image 8x8 with moderate contrast [22].

4.2.1 Setup

First, to start the experiment, the pixel values of the images were converted to a power scale (dBm), maximizing the power range available from the C band lasers. The ranges used in the experiment are listed in Table 6 and Table 7 for each image and setup.

Image Unit		4x4 Images			8x8 Image
		Moderate contrast	High contrast	Low contrast	
Pixel	Lower value	55	53	161	30
	Higher value	202	223	162	175
dBm	Lower value	1.13	2.49	6.42	2.7
	Higher value	7.4	7.6	7.1	7.02

Table 6: Power range used with the 3dB coupler setup.

Image Unit		4x4 Images			8x8 Image
		Moderate contrast	High contrast	Low contrast	
Pixel	Lower value	55	53	161	30
	Higher value	202	223	162	175
dBm	Lower value	4.88	4.16	6.99	5.32
	Higher value	7.77	7.8	7.72	7.77

Table 7: Power range used with the Waveshaper setup.

Secondly, two different setups were used to compare results. One of the setups (Figure 35 and Figure 36) was assembled with a regular one input, two output 3dB coupler with 3.5 dB in each Port. The second setup (Figure 37 and Figure 38) was assembled with a Finisar Waveshaper 4000s, working as a one input, two output 3dB coupler with 4.5dB loss in each port.

The Finisar Waveshaper 4000s is a very important component, because with the 3dB Couplers, it is only possible to obtain the Scaling image of the Haar wavelet

transform by averaging the inputs. But with the Waveshaper, if the experiment working as a 3dB Coupler is successful (obtained images similar to the originals), it will be possible to implement all the Haar wavelet transform, as well as to extract not only the Scaling image, but also the three details images.

The rest of the components were common to both of the setups:

- 2 Polarization controllers;
- 1 Attenuators;
- 1 External Cavity Laser (ECL) in the C band (1550 nm);
- 1 Tunable Laser Source (TLS) in the C band (1550 nm);
- 1 Power meter.

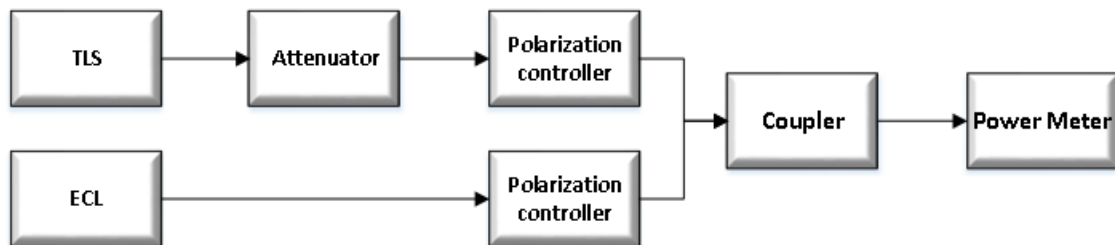


Figure 35: Setup with 3dB coupler.

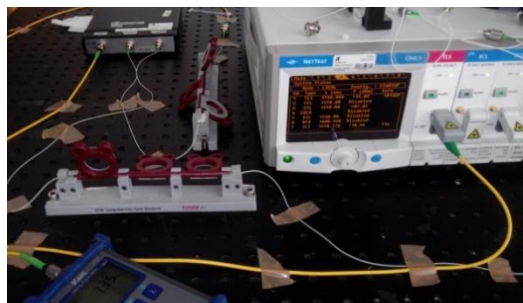


Figure 36: Photography of the 1550 nm setup with 3dB coupler.

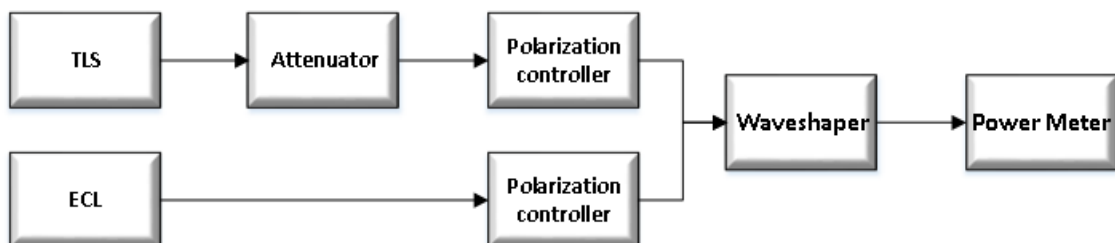


Figure 37: Setup with Waveshaper.

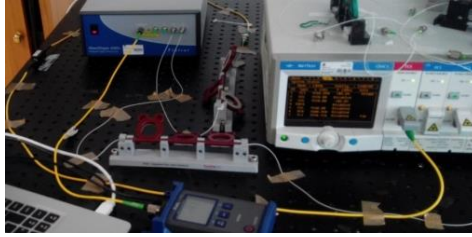


Figure 38: Photography of the 1550 nm setup with Waveshaper.

Next, with the values of the pixel converted to the power scale (dBm), the same steps from chapter 4.1.1, to obtain the final LL component (Scaling image of the Haar wavelet transform) were also used.

4.2.2 Results

To analyze the results, the same five different parameters from chapter 4.1.2 were used.

	Coupler		Waveshaper	
	Insertion Loss (Pixel)	Average Standard Deviation (Pixel)	Insertion Loss (Pixel)	Average Standard Deviation (Pixel)
4 x 4 Moderate contrast	1.03±0.05	0.15	0.38±0.19	0.09
4x4 High contrast	1.02±0.03	0.02	0.55±0.17	0.07
4x4 Low contrast	1.00±0	0	0.94±0.01	0.59
8x8 Image	1.13±0.22	0.05	0.38±0.27	0.02

Table 8: Insertion loss and average Standard Deviation comparison.

From Table 8, analyzing the obtained values of the parameter Insertion Loss, it is possible to say that in the case of the Coupler, the images are expected to be very similar to the original. Where the image 4x4 with Low contrast is the most similar and the 8x8 Image is the one more different from the original but still very much alike.

In the case of the Waveshaper, judging from obtained values of the parameter Insertion Loss, the images are expected to be a little different from the originals since the Insertion Loss is much smaller than one with a little bit of deviation. The most similar image to the originals is expected to be the image 4x4 with Low contrast and the one more different from the original is expected to be the 8x8 image.

Looking at the value of the Average Standard Deviation, it is possible to say that in the case of the 1550 nm wavelength, the results are not significantly affected by the operation of disconnecting and connecting the fibers, where the higher obtained error is about 1 pixel.

	Coupler		Waveshaper	
	MSE (pixel)	PSNR (dB)	MSE (pixel)	PSNR (dB)
4 x 4 Moderate contrast	7.5	39.4	19785.5	5.2
4 x 4 Moderate contrast with IL	7.75	39.2	1840.5	15.5
4x4 High contrast	16.5	35.9	7820.8	9.2
4x4 High contrast with IL	8.75	38.7	1822.3	15.5
4x4 Low contrast	0.5	51.1	122.5	27.2
4x4 Low contrast with IL	0.5	51.1	1	48.1
8x8 Image	61.5	30.2	23158.4	4.5
8x8 Image with IL	66.6	29.9	2101.7	14.9

Table 9: MSE and PSNR comparison.

From Table 9, it is possible to confirm most of the deductions made in Table 8, where the Coupler produces better results than the Waveshaper. The only deduction that was not confirmed from Table 8 was the quality of the images obtained from the Waveshaper, where from the high obtained values of MSE and

low values of PSNR, it is expected that the images turn out to be very different from the original. The only image obtained from the Waveshaper that might be similar to the original is the 4x4 with Low contrast, where the obtained image multiplied by the Insertion Loss (IL) will be very similar to the original.

4.2.3 Image comparison

In this chapter, the images will be compared using the human eye perception, comparing the theoretical Scaling image with each one of the obtained Scaling images, the same way as in chapter 4.1.3.

4.2.3.1 4x4 Image with moderate contrast:



Figure 39: Theoretical Scaling image [22].

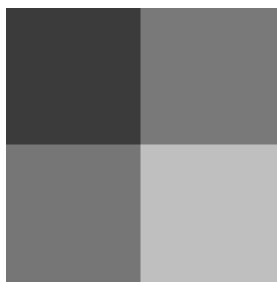


Figure 40: Obtained Scaling image from the 3dB coupler with IL.



Figure 41: Obtained Scaling image from the 3dB coupler without IL [22].

Comparing the theoretical Scaling image (Figure 39) with the obtained images (Figure 40 and Figure 41), it is possible to say that the images obtained with the Coupler are a little bit lighter than the theoretical one, but the contrasts remain, confirming the values of the MSE and PSNR from chapter 4.2.2.

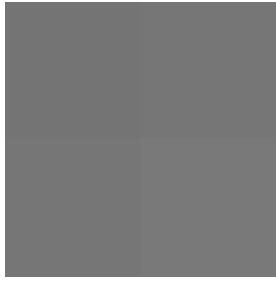


Figure 42: Obtained Scaling image from the Waveshaper with IL.

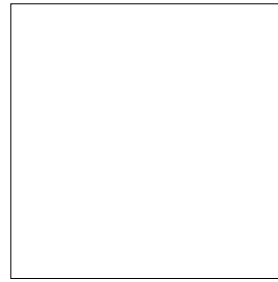


Figure 43: Obtained Scaling image from the Waveshaper without IL.

From Figure 42 and Figure 43, the deductions made from the quality parameters on chapter 4.2.2 are confirmed, where the images obtained with the Waveshaper are very different from the theoretical one (Figure 39), resulting in a very high MSE and a very low value for the PSNR.

4.2.3.2 4x4 Image with high contrast:



Figure 44: Theoretical Scaling image [22].



Figure 45: Obtained Scaling image from the 3dB coupler with IL.



Figure 46: Obtained Scaling image from the 3dB coupler without IL [22].

Comparing the theoretical Scaling image (Figure 44) with the obtained images (Figure 45 and Figure 46), even increasing the contrast in the image, the deductions made in the previous chapter 4.2.3.1 remain, where the images

obtained with the Coupler are very similar to the theoretical image, just a little bit lighter.

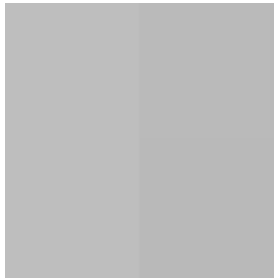


Figure 47: Obtained Scaling image from the Waveshaper with IL.

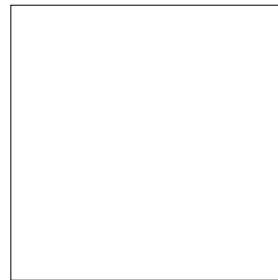


Figure 48: Obtained Scaling image from the Waveshaper without IL.

With the Waveshaper, Figure 47 and Figure 48 remain very different from the theoretical one(Figure 44), improving when multiplying the obtained image by the IL, making it possible to see some contrast, but still very different from the expected.

4.2.3.3 4x4 Image with low contrast:



Figure 49: Theoretical Scaling image [22].



Figure 50: Obtained Scaling image from the 3dB coupler with IL.

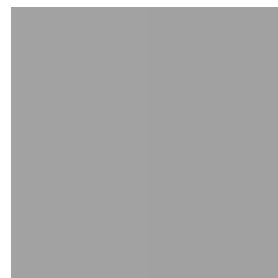


Figure 51: Obtained Scaling image from the 3dB coupler without IL [22].

Comparing the theoretical Scaling image (Figure 49) with the obtained images (Figure 50 and Figure 51), when the Coupler was used and the contrast in the image was reduced, they look very much alike as the theoretical one, proving the deduction obtained in chapter 4.2.2, where the obtained image with Low contrast was expected to be the most similar.



Figure 52: Obtained Scaling image from the Waveshaper with IL.



Figure 53: Obtained Scaling image from the Waveshaper without IL.

In the case of the Waveshaper, the deductions made in chapter 4.2.2 are also proven, where Figure 52 and Figure 53 are very similar to the theoretical one, only a little bit darker, increasing the value of the MSE.

4.2.3.4 8x8 Image with moderate contrast:

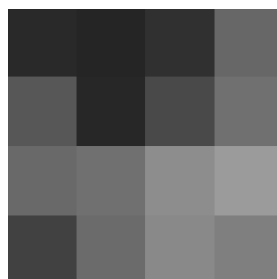


Figure 54: Theoretical Scaling image [22].

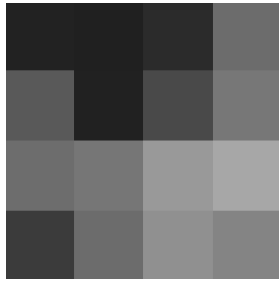


Figure 55: Obtained Scaling image from the 3dB coupler with IL.

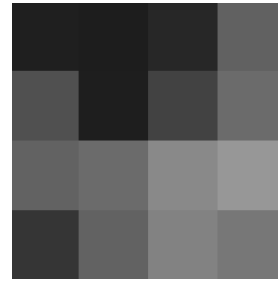


Figure 56: Obtained Scaling image from the 3dB coupler without IL [22].

In the case of the images 8 by 8 pixel obtained with the Coupler, comparing the theoretical Scaling image (Figure 54) with the obtained images (Figure 55 and Figure 56), even increasing the number of pixel of the image, they are very similar to the theoretical one, more than what was expected from the quality parameters obtained in chapter 4.2.2.



Figure 57: Obtained Scaling image from the Waveshaper with IL.

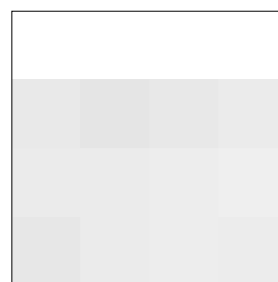


Figure 58: Obtained Scaling image from the Waveshaper without IL.

From the images obtained with Waveshaper, they prove the deductions made in the previous chapter, where Figure 57 and Figure 58 are very different from the theoretical one (Figure 54), explaining the high values of the MSE and PSNR in chapter 4.2.2. From these two images, the one more similar to the theoretical one is still the one multiplied by the IL.

4.2.4 Discussion of results

The laboratory experiment in the C band (1550 nm wavelength) has proven to be very successful in obtaining the Scaling image with the 3dB Coupler, given very

good results in images with different values of contrast, even without considering the loss in the components, which means, not considering the IL.

In the case of the Waveshaper, the results have proven to have a lot of error when images with contrast are considered and when the most similar images are the ones whose loss in the components is compensated with the IL. For images with low contrast, the Waveshaper has given reasonable results, even with a little bit of error but still similar from the expected ones.

One of the reasons for these results with Waveshaper is that, since the power scale is a logarithmic scale, the pixel scale is a linear scale and the device has significant value of loss in its ports (4.5dB of loss in each processing operation added 2 times for the operation on the rows and on the columns). Due to this amount of loss, the input values need to be very high to compensate the 9dB loss just in the Waveshaper (without considering the loss in the fibers and other components) to maintain the input power of the Waveshaper in the positive side of the Logarithmic scale.

Then, a summary manner of the previous deductions:

- The setup that introduced better results considering all the parameters was the 1x2 3dB Coupler due to its low amount of loss. In this case, to simplify the circuit, the value of the Insertion Loss does not have to be considered, since the difference between with or without is not significant enough;
- Adding the Insertion Loss to the images, in the case of the Waveshaper, it may produce better results, decreasing the MSE. However, in other images, it may introduce more error, as seen in the image with 4 by 4 pixels with moderate contrast and in the 8 by 8 pixels image, increasing the MSE value.

Chapter 5: Optical Haar transform design

5.1 Phoenix OptoDesigner

Phoenix Software OptoDesigner is a platform for design, simulation and mask layout of photonic integrated circuits [23]. The modular approach, which includes the programs, MaskEngineer, FieldDesigner, OptoDesigner and FlowDesigner offers the advantage of a tailor-made or user defined software package with flexibility to meet every individual's specific needs.

In this case, FieldDesigner was used to study the modes propagation in both single and coupled waveguides. However, in FieldDesigner, only the cross-section of the waveguide is visible. Therefore, it is not possible to draw a whole circuit, the user only simulates an element at a time.

To study the whole circuit based on the Beam Propagation Method, the program OptoDesigner will be used, in which the different parameters will be analyzed and then optimize the circuit for the desired output parameters.

5.2 3dB asymmetric coupler design

OptoDesigner was used to design and simulate the coupler that is represented in Figure 59. This is a 3 dB asymmetric optical coupler, also known in literature as Magic-T, whose scattering matrix was already shown in Figure 4. The design was performed based on the Coupled Mode Theory (CMT) and the information given in [18].

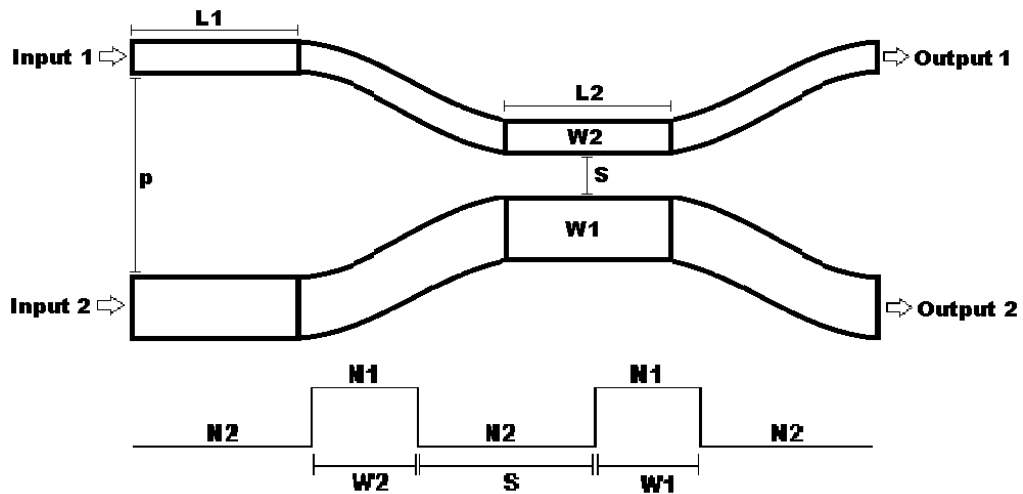


Figure 59: 3 dB asymmetric coupler geometry and design [22].

The device was designed to have the specifications of a monomode asymmetric coupler in the visible spectral region, and optimized for the wavelength of 635 nm (Red). In order to simplify the process and taking into account materials with a low production cost, the considered materials were SU-8-3005 (Microchem) for the cladding and a mixture of SU-8-3005-Epoclad (Microchem) (14 % in volume) for the core of the waveguide. For the optimized device, a maximum coupling ratio of 50% occurs when the optical input is injected in the wider waveguide (W_1), with the resulting outputs signals having a phase shift of 0 degrees, when compared with the input signal. When the optical signal is injected in the narrower waveguide (W_2), the resulting signal at output of the waveguide W_2 must have a phase difference of 180 degrees, while the optical signal at the output of W_1 should have a null phase shift, in relation to the input signal.

To fulfill these specifications, the following parameters, which are specified in Figure 59 were optimized by using the beam propagation method in OptoDesigner:

- Refractive Index Contrast (N_1 and N_2): contrast is defined by the materials technology used to fabricate the device. The larger the contrast, the stronger is the confinement of light within the waveguide, resulting in less coupling between the two coupler arms. Moreover, materials choice influences the overall size of waveguides for desired single-mode propagation. In this case, the materials SU-8-3005 (Microchem), for the cladding, and a mixture of SU-

8-3005-Epoclad (Microchem) (14 % in volume), for the core, show a Refractive Index of 1.5681 and 1.5701, respectively;

- Separation between waveguides (S): this parameter is fundamental to control the coupling strength. More separation means less coupling between the two coupler arms. This is the key operation able to set the coupling at a maximum of 50%;
- Waveguides widths ($W1$ and $W2$): difference between widths controls the phase difference (propagation constants) between coupled modes, and thus the length corresponding to the π phase difference between output waves;
- Couplers length (L): since the waveguides have different widths, the modes will propagate with distinct propagation constants; therefore, for a specific length, the phase will suffer different changes in each waveguide. L definition includes arms' length, but in the optimization, only the straight coupling region ($L2$) length is changed;
- Pixel separation (p): the distance between the two input ports/output ports corresponds to the physical pixel separation.

First, taking into account the materials used and the refractive index contrast, the first parameters to optimize were the waveguide widths ($W1$ and $W2$) and the materials effective indices ($N1$ and $N2$). As it was stated before, the OptoDesigner is the Phoenix Software tool that allows simulating the entire asymmetric coupler. However, it implies the knowledge of the effective indices. Since only the refractive indices were known, some simulations were performed in FieldDesigner in order to get the effective indices. The wavelength was set to 635 nm, and the widest ($W1$) and the narrowest ($W2$) waveguides widths to 4.5 μ m and 4 μ m, respectively. The resulting effective indices are listed in Table 10. Note that, each width is lower than the cutoff width for the second mode, and it is guaranteed that only TE0 and TE1 are propagated in the coupled waveguides.

Secondly, with the wavelength and parameters $N1$, $N2$, $W1$ and $W2$ already fixed, the parameters S , p , $L1$ and $L2$ were optimized. In OptoDesigner, with the input in the narrower waveguide ($W2$), fixing p to the minimum distance, which still prevents coupling between 2 parallel couplers, and applying signal to the narrowest waveguide input ($W2$), the aim was to find the S value, which allowed reaching a

maximum coupling of 50% (half of the power inserted in the input in each one of the outputs).

Finally, with a coupling of 50%, the parameters $L2$ and $L1$ were optimized to obtain the desired phase difference. After simulating these steps repeatedly in OptoDesigner, and based on the values from Table 10, the output values of power and phase listed in Table 11 were obtained.

Parameter	Value
S (μm)	2.324
p (μm)	29.75
L2 (μm)	100
L1 (μm)	18.2
W1 (μm)	4.5
W2 (μm)	4
N1	1.5695
N2	1.5678

Table 10: Parameters for the simulated 3dB asymmetric coupler.

Output \ Input		Wider waveguide	Narrowed waveguide
Narrowed waveguide	Power (mW)	0.49	0.49
	Phase ($^\circ$)	1.03	-176.91
Wider waveguide	Power (mW)	0.49	0.49
	Phase ($^\circ$)	-0.48	1.60

Table 11: Output values from the simulated 3db asymmetric coupler [22].

5.3 Optical Haar transform design

For the optical Haar transform design, the desired specifications were:

- Average value in one of the outputs of the amount of power inserted in the 4 inputs with zero degree phase shift;
- The power difference between the average value and inputs in the remaining outputs.

To design and simulate this structure in OptoDesigner, the 3dB asymmetric coupler represented in Figure 59 was used as the baseline model, with the parameters from Table 10.

With the 3dB asymmetric coupler optimized, the optical Haar transform was designed using three concatenate 3dB asymmetric couplers: two 3dB asymmetric couplers in parallel and a third one, whose inputs are connected to the output arms of the previous asymmetric couplers.

The schematic for the optical Haar transform is described in Figure 60 and its parameters are listed in Table 12.

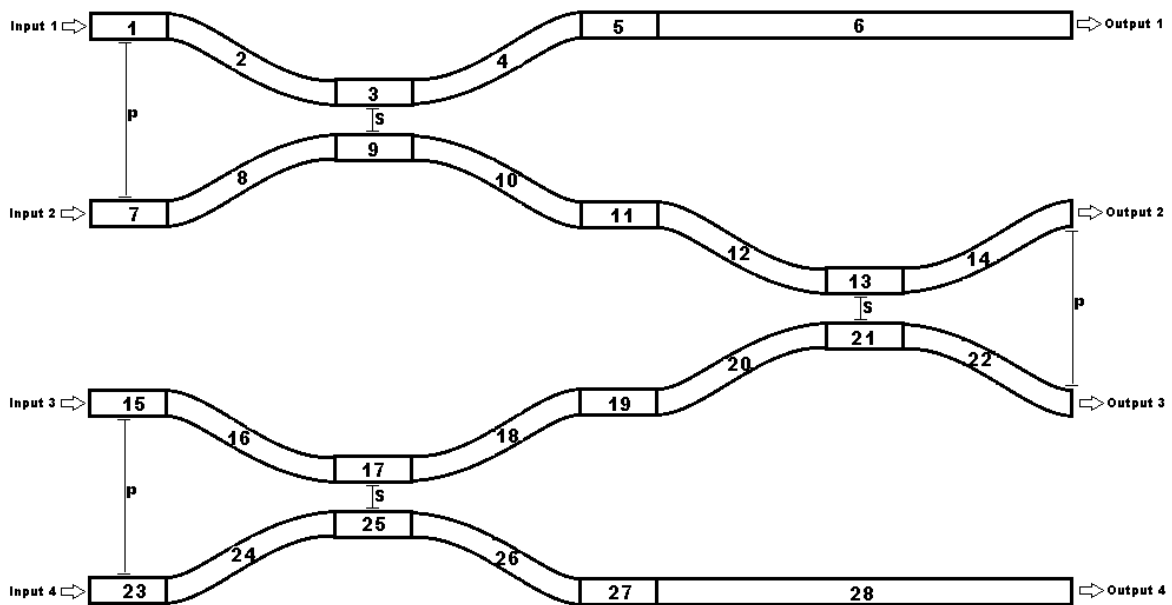


Figure 60: Schematic of the optical Haar transform [22].

Element Number	Element type	Initial Width (μm)	Final Width (μm)	Length (μm)
1 / 19 / 23	Linear Taper	4.5	4	18.2
7 / 11 / 15	Linear Waveguide	4.5	4.5	18.2
5 / 27	Linear Waveguide	4	4	18.2
2 / 4 / 20 / 22 / 24 / 26	S-Bend Sine	4	4	1800
8 / 10 / 12 / 14 / 16 / 18	S-Bend Sine	4.5	4.5	1800
3 / 21 / 25	Linear Waveguide	4	4	100
9 / 13 / 17	Linear Waveguide	4.5	4.5	100
6 / 28	Linear Waveguide	4	4	3718.2

Table 12: Parameters for the optical Haar transform schematic.

5.4 Discussion of results

The optical Haar transform exposed in the previous subsection 5.3 was simulated for five different scenarios, in which different input powers were applied to the mentioned structure. The respective Input power and the theoretical value that should be obtained in each output of the device represented in Figure 60 are listed in Table 13. The theoretical value that should be obtained and the output value obtained in the four outputs of the same device are listed in Table 14.

The Output Port was calculated with Equation (5.1), where *Power* denotes the amount of power in the output of one of the arms and phase denotes the corresponding *Phase* in that output arm:

$$\mathbf{Output\ port} = \mathbf{Power} * \mathbf{cos(Phase)} \quad (5.1)$$

Figure 61 and Figure 62 shows the resulting field propagation and phase distribution when an input signal of 1mW and zero degree phase is inserted in the four inputs, which corresponds to the Simulation 1 listed in Table 13 and Table 14.

Simulation Parameter		Simulation				
		1	2	3	4	5
Input port (mW)	1	1	1	0.8	0.5	0.1
	2	1	0.8	1.2	0.5	0.9
	3	1	1.2	1	0.5	0.3
	4	1	1	1	0.5	0.7
Theoretical output port	1	0	0.1	-0.1	0	-0.3
	2	1	1	1	0.5	0.5
	3	0	-0.1	0	0	0
	4	0	0	-0.1	0	-0.1

Table 13: Input and theoretical output value in each port of the optical Haar transform.

Simulation Parameter		Simulation				
		1	2	3	4	5
Theoretical output port	1	0	0.1	-0.1	0	-0.3
	2	1	1	1	0.5	0.5
	3	0	-0.1	0	0	0
	4	0	0	-0.1	0	-0.1
Obtained output port	1	0	0	0.02	0	0.14
	2	3.99	3.97	3.97	2	1.75
	3	0	-0.01	0	0	0
	4	0	0	0	0	-0.03

Table 14: Theoretical and output value in each port of the optical Haar transform.

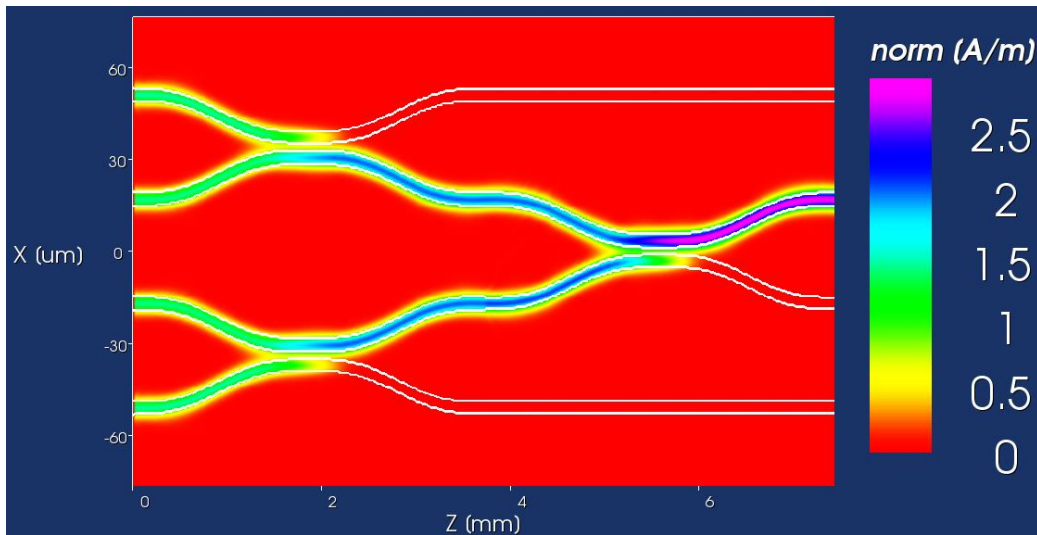


Figure 61: Power propagation along the optical Haar transform schematic for Experiment 1 [22].



Figure 62: Phase propagation along the optical Haar transform schematic for Experiment 1 [22].

From Table 14, it is possible to verify a relation between the *Theoretical output port 2* and the *Obtained output port 2*. Instead of having in the *Obtained output port 2* the average value that corresponds to the *Theoretical output port 2*, the sum of the four inputs is observed. With an attenuator in the output that decreases his value by a constant of 4, the desired *Theoretical output port 2* of 1mW is obtained in the *Obtained output port 2*.

In addition, it is confirmed that when the power is equitably distributed in the four inputs (Experiment 1 and Experiment 4), practically all of the power from the inputs is propagating towards the *Obtained output port 2*. Since the expected power in the output port was 4mW for Experiment 1, one can conclude that when an attenuator is added in *Obtained output port 2*, in the worst case (when the output value in the port is higher), the obtained result is very satisfactory (relative error minor than 0.25%).

In the other cases, when the power should be distributed to the remaining outputs (Experiment 2, Experiment 3 and Experiment 5), this device has proven to show a significant amount of error, only being able to deliver successfully the output of the Scaling image (*Obtained output port 2*).

Chapter 6: Conclusion and future work

In this thesis, an all-optical system based on the Haar Wavelet transform was presented, capable of obtaining significant compression ratio with low loss of quality in image files. Several methods can be applied, depending on which type of image it is meant to compress. The types of images whose size is not important and for which high compression ratio is required, lossy compression can be advantageous. The lossless compression should be used when all the details of the image are important, obtaining lower level of compression but gaining in image quality. Also, additional compression can be added, reducing the number of symbols by thresholding or quantization, increasing the image transmission speed on an optical channel.

In the laboratory, it was noted that, in terms of lossy compression, the 3dB coupler for the 1550 nm wavelength, has proven to be the best setup comparing with the Waveshaper, providing images with high compression ratio and quality. The Waveshaper setup, despite showing worst results than the 3dB Coupler, was also important to analyze because with it, it is possible to obtain not only the Scaling image of the Haar Transform but also the Details images, generating a lossless compression method instead of a lossy compression method like the one used in the 3dB coupler. With these results, it is possible to confirm that with this setup, the errors obtained are considerable, making it impossible to obtain the original image and generate a lossless compression method.

Nevertheless, the design of the optical Haar transform was presented, showing low values of loss when the power inserted in the inputs are the same, making it possible to obtain an optical device that performs the Haar wavelet transform. When the Power in the inputs has different values, this device has shown to provide a significant amount of error delivering the output power in the outputs corresponding to the Details images, only providing successfully the power in the output of the Scaling image.

For future work, different setups and different wavelengths can be used to apply the Haar wavelet transform, reducing the amount of error and increasing the quality of the image obtained.

In addition, several more methods can be used to compress an image. A simple method is to apply the Haar transform (or a different transform), then a threshold or quantization to the Scaling image and transmit that image to obtain a higher amount of compression and data transmission. Another more elaborated method is to implement a compression method using the Haar wavelet transform and algorithms, method used for example, in the JPEG200 standard.

In this research field, there is still a lot of work to develop and new devices and transforms being created every day, making it possible to obtain higher levels of image quality and compression.

References

- [1] P. N. Topiwala, "Wavelet image and video compression", Kluwer Academic, 1998.

- [2] C. Hangen, K. Khan, M. Ciobo, J. Miller, D. Wall, H. Evans, A. Yadav, "Big Data and the Creative Destruction of Today's Business Models", A.T. Kearney, 2013.

- [3] G. Blelloch, "Introduction to Data Compression", Computer Science Department, Carnegie Mellon University, 2013.

- [4] A. E. Siegman, "Fiber Fourier optics", Optics letters, 2001.

- [5] S. Jha, U. Khankhoje, A. Dixit, "Propagation in Optical Fibers using Wavelets", Wavelets Application Assignment, 2004.

- [6] C. N. Doukas, I. Maglogiannis, G. Kormentzas, "Medical Image Compression using Wavelet Transform on Mobile Devices with ROI coding support", Engineering in Medicine and Biology 27th Annual Conference, IEEE, pp. 3779-3784, 2005.

- [7] S. Lévêque-Fort, "Three-dimensional acousto-optic imaging in biological tissues with parallel signal processing", Applied Optics, Optical Society of America, vol. 40, pp. 1029-1036, 2000.

- [8] A. Alfalou, C. Brosseau, "Optical image compression and encryption methods", Advances in Optics and Photonics 1, Optical Society of America, pp. 589-636, 2009.

- [9] A. Skodras, C. Christopoulos, T. Ebrahimi, "The JPEG 2000 Still Image", Signal Processing Magazine, IEEE, pp. 36-58, 2001.

- [10] J. Li, S. Lei, "An embedded still image coder with rate-distortion optimization", Transactions on Image Processing, IEEE, vol. 8, pp. 913-924, 1999.
- [11] G.M. Davis, A. Nosratinia, "Wavelet-based Image Coding: An Overview", Applied and Computational Control, Signals and Circuits, vol. 1, 1998.
- [12] J.S. Walker, "Wavelet-Based Image Compression", Wisconsin, USA: Transform and Data Compression. A Primer on Wavelets and Their Scientific Applications, 1999.
- [13] J. Kerekes. (2014, 2 June) "Image data Compression", [Online]. Available: <http://www.grss-ieee.org/technical-resources-2/image-data-compression/>.
- [14] G. Strang, T. Nguyen, "Wavelets and Filter Banks", SIAM, 1996.
- [15] Thyagarajan, K. S., "Still Image and Video Compression with MATLAB", John Wiley & Sons, 2011.
- [16] G. Parca, P. Teixeira, A. Teixeira, "All-optical image processing and compression based on Haar wavelet transform", Applied Optics, Optical Society of America, vol. 52, 2013.
- [17] G. Parca, P. Teixeira, A. Teixeira, "3D interferometric integrated passive scheme for all optical transform", 14th International Conference on Transparent Optical Networks, IEEE, 2012.
- [18] A. Takagi, K. Jinguji, M. Kawachi, "Design and fabrication of broad-band silica-based optical waveguide couplers with asymmetric structure," J. Quantum Electron. 28, IEEE, pp. 848-855, 1992.

- [19] T. Mitsumoto, Y. Naito, "Dependence of the output phase difference on the asymmetry of 3 dB directional couplers," J. Lightwave Technol. 8, pp. 1571-1576, 1990.
- [20] Z. Wang, A.C. Bovik, "A universal image quality index", Signal Processing Letters, IEEE, vol. 9, pp. 81-84, 2002.
- [21] A. Majumder, "Contrast Enhancement of Multi-Displays Using Human Contrast Sensitivity", Computer Society Conference on Computer Vision and Pattern Recognition, IEEE, vol. 2, pp. 377-382, 2005.
- [22] L. Almeida, A. Teixeira, G. Parca, N. Kumar, A. Lopes, A. Tavares, A. Shahpari, "All-Optical Image Compression Processing Based on Integrated Optics", 16th International Conference on Transparent Optical Networks, IEEE, 2014.
- [23] Phoenix Software, "User Manual OptoDesigner", Phoenix BV, version 4.8.2, 2013.

Attachments



Figure 63: TIF 1 - Original image.



Figure 64: TIF 1 - Haar transform image.

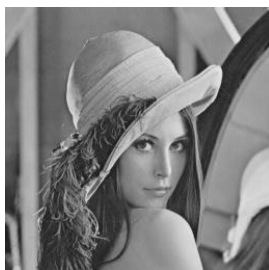


Figure 65: TIF 1 - Scaling image of the Haar transform.



Figure 66: TIF 2 - Original image.



Figure 67: TIF 2 - Haar transform image.



Figure 68: TIF 2 - Scaling image of the Haar transform.

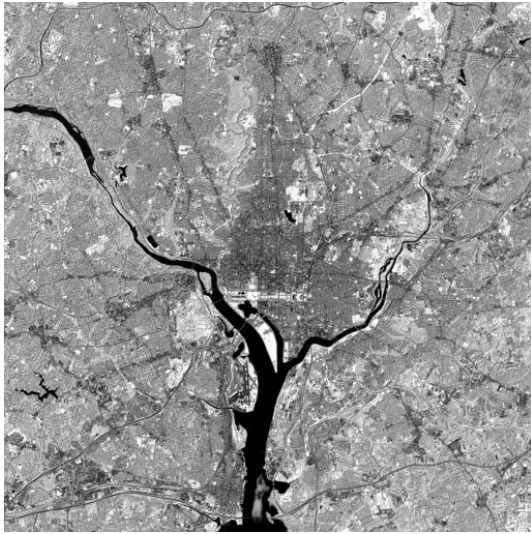


Figure 69: TIF 3 - Original image.

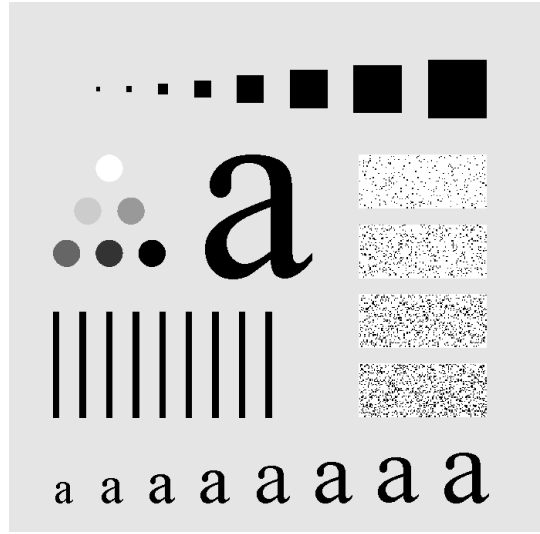


Figure 72: TIF 4 - Original image.

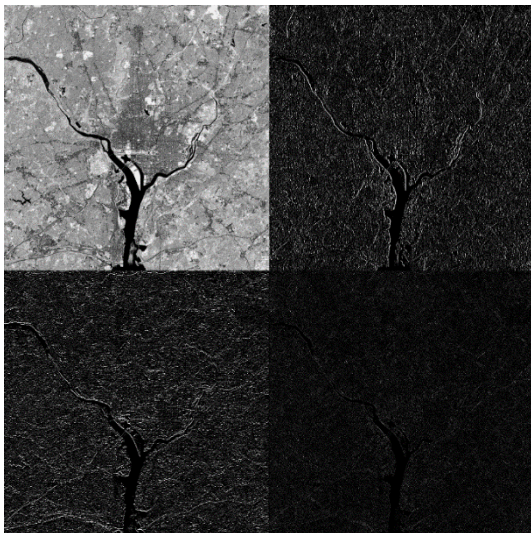


Figure 70: TIF 3 - Haar transform image.

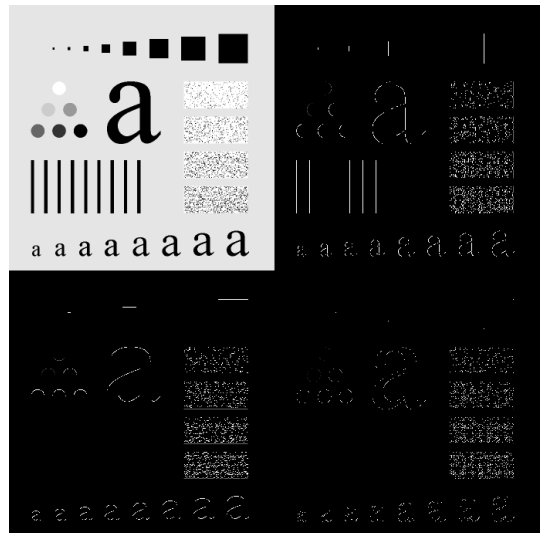


Figure 73: TIF 4 - Haar transform image.

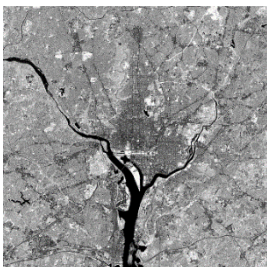


Figure 71: TIF 3 - Scaling image of the Haar transform.

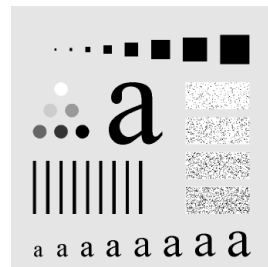


Figure 74: TIF 4 - Scaling image of the Haar transform.



Figure 75: JPEG 1 - Original image.



Figure 78: JPEG 2 - Original image.

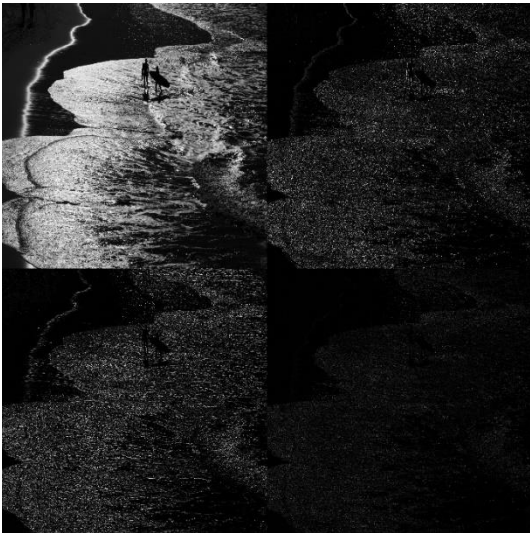


Figure 76: JPEG 1 - Haar transform image.



Figure 79: JPEG 2 - Haar transform image.

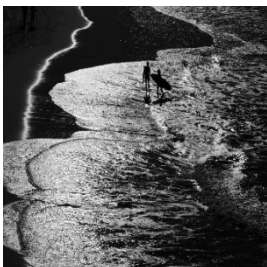


Figure 77: JPEG 1 - Scaling image of the Haar transform.

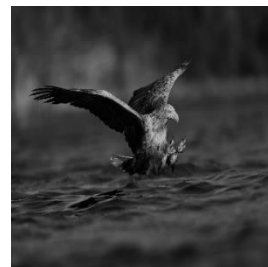


Figure 80: JPEG 2 - Scaling image of the Haar transform.



Figure 81: JPEG 3 - Original image.

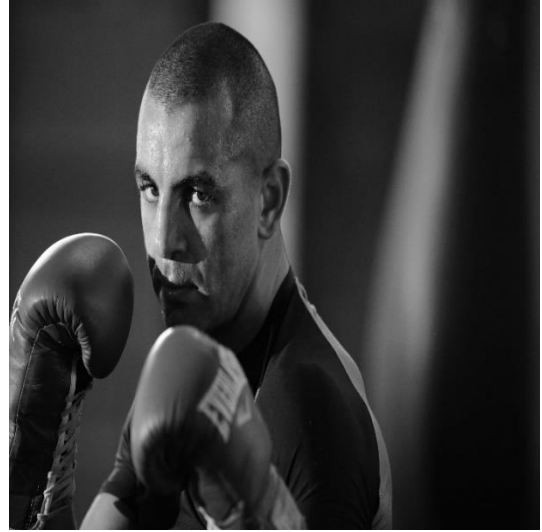


Figure 84: JPEG 4 - Original image.



Figure 82: JPEG 3 - Haar transform image.

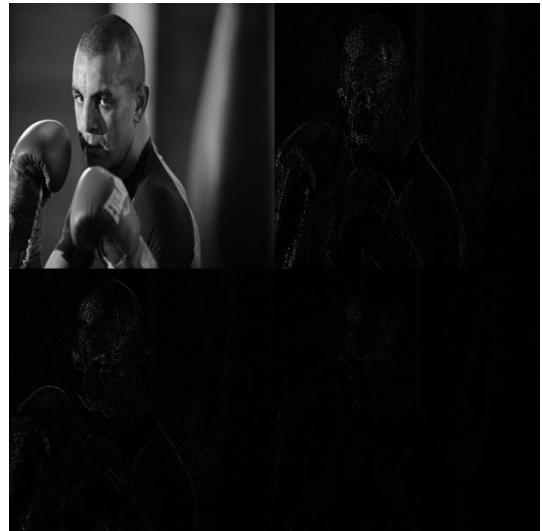


Figure 85: JPEG 4 - Haar transform image.



Figure 83: JPEG 3 - Scaling image of the Haar transform.

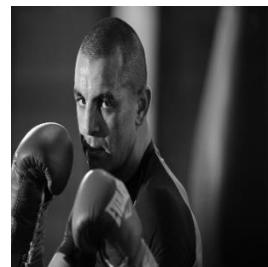


Figure 86: JPEG 4 - Scaling image of the Haar transform.



Figure 87: BMP 1 - Original image.

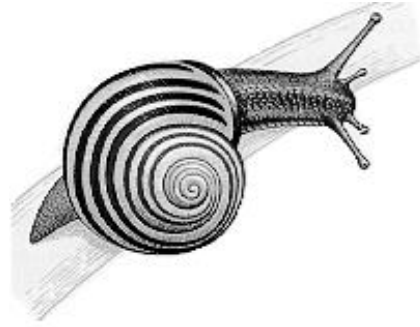


Figure 90: BMP 2 - Original image.

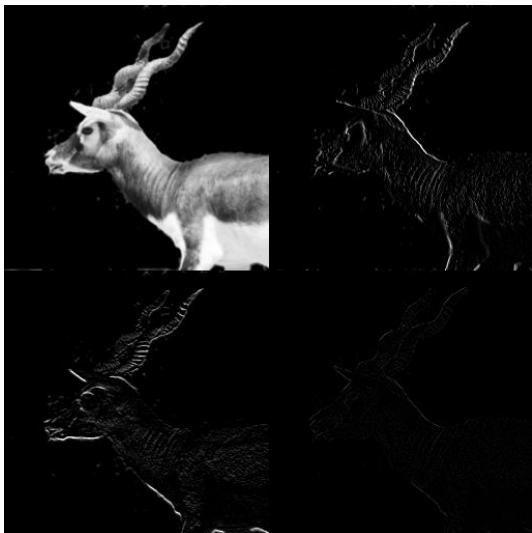


Figure 88: BMP 1 - Haar transform image.

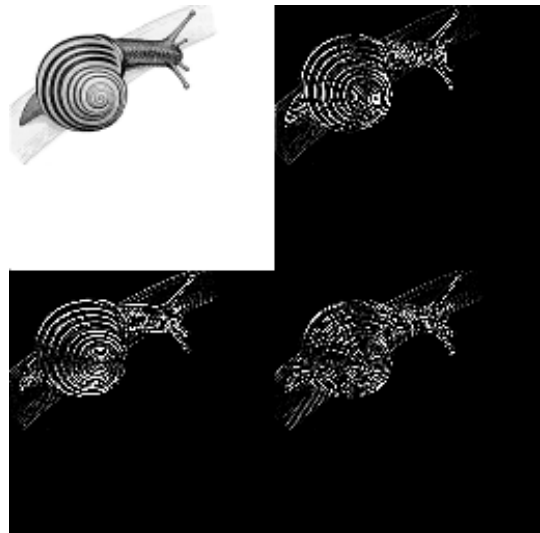


Figure 91: BMP 2 - Haar transform image.

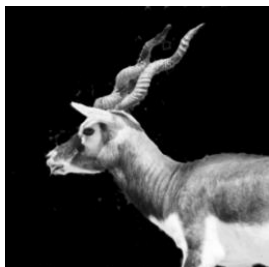


Figure 89: BMP 1 - Scaling image of the Haar transform.



Figure 92: BMP 2 - Scaling image of the Haar transform.

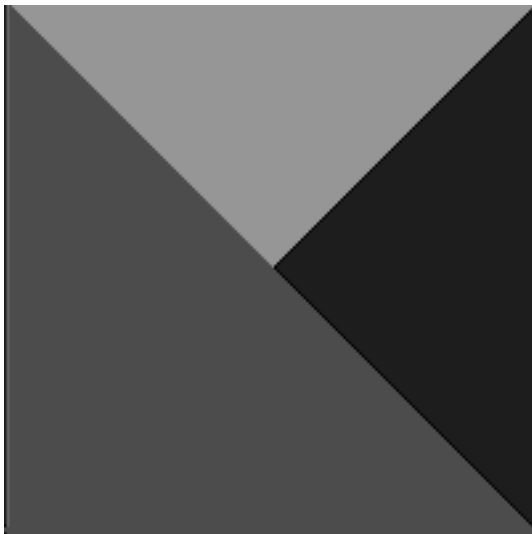


Figure 93: BMP 3 - Original image.



Figure 96: BMP 4 - Original image.



Figure 94: BMP 3 - Haar transform image.



Figure 97: BMP 4 - Haar transform image.



Figure 95: BMP 3 - Scaling image of the Haar transform.



Figure 98: BMP 4 - Scaling image of the Haar transform.



Figure 99: PNG 1 - Original image.



Figure 102: PNG 2 - Original image.



Figure 100: PNG 1 - Haar transform image.



Figure 103: PNG 2 - Haar transform image.

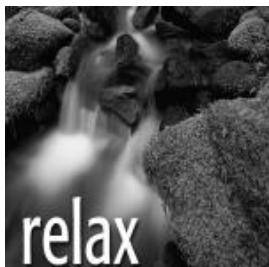


Figure 101: PNG 1 - Scaling image of the Haar transform.



Figure 104: PNG 2 - Scaling image of the Haar transform.



Figure 105: PNG 3 - Original image.



Figure 108: PNG 4 - Original image.

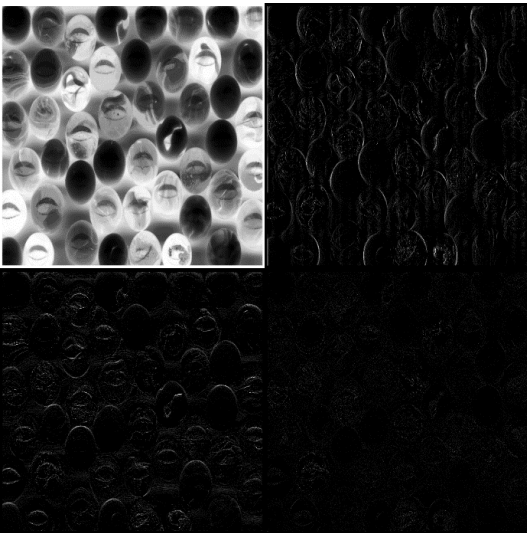


Figure 106: PNG 3 - Haar transform image.

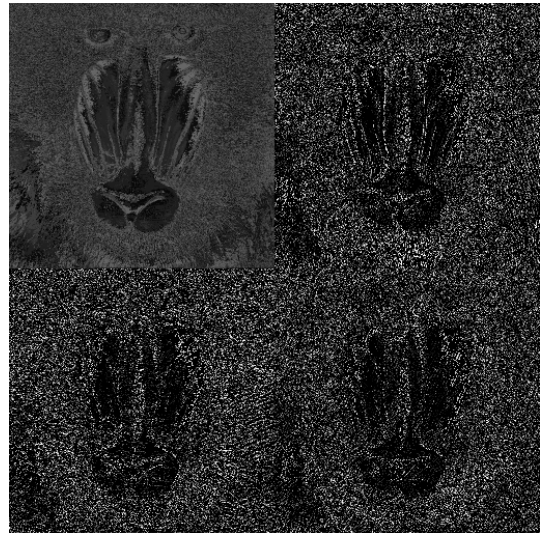


Figure 109: PNG 4 - Haar transform image.



Figure 107: PNG 3 - Scaling image of the Haar transform.

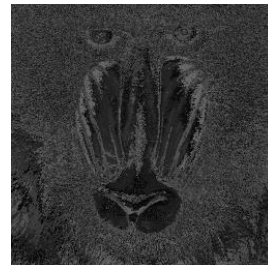


Figure 110: PNG 4 - Scaling image of the Haar transform



Figure 111: Haar inverse transform from image TIF 1 after a threshold level of 0



Figure 113: Haar inverse transform from image TIF 1 after a threshold level of 8



Figure 112: Haar inverse transform from image TIF 1 after a threshold level of 4



Figure 114: Haar inverse transform from image TIF 1 after a threshold level of 16



Figure 115: Haar inverse transform from image TIF 1 after a threshold level of 32



Figure 117: Haar inverse transform from image TIF 1 after a threshold level of 128



Figure 116: Haar inverse transform from image TIF 1 after a threshold level of 64



Figure 118: Haar inverse transform from image TIF 1 after a quantization level of 1



Figure 119: Haar inverse transform from image TIF 1 after a quantization level of 2



Figure 121: Haar inverse transform from image TIF 1 after a quantization level of 10



Figure 120: Haar inverse transform from image TIF 1 after a quantization level of 5



Figure 122: Haar inverse transform from image TIF 1 after a quantization level of 20



Figure 123: Haar inverse transform from image TIF 1 after a quantization level of 50